A Comparison of a GCM Simulation of the Seasonal Cycle of the Atmosphere With Observations
Part I: Mean Fields and the Annual Harmonic

David M. Straus
Laboratory for Atmospheres
NASA/Goddard Space Flight Center
Greenbelt, Maryland 20771
and
J. Shukla
Center for Ocean-Land-Atmosphere Interactions
Department of Meteorology
University of Maryland
College Park, Maryland 20742

[Original manuscript received 16 June 1987; in final form 22 April 1988]

ABSTRACT *The seasonal cycle of the GLAS/U of Maryland GCM is analysed in terms of the behaviour of the monthly and seasonal mean fields and the structure of the annual harmonic. (The stationary and transient eddies are treated in a companion paper.)*

Both polar regions at upper levels are much too cold in the annual mean, leading to excessive zonal winds above 200 mb. The problem is present in all seasons, but is most severe in local winter. A compensating belt of warm temperatures at lower latitudes is found. It is argued that the inclusion of gravity wave drag is not necessarily the solution to this problem.

The simulated annual harmonics of Northern Hemisphere sea-level pressure and 200-mb heights are realistically intense over the eastern continents and weak over the eastern oceans. Problems in the simulation include the anomalously deep Aleutian low and the low values of the height over Europe, both occurring in winter.

The simulation of the annual harmonic in sea-level pressure and 200-mb heights in the Southern Hemisphere is realistic. The GCM fails to show the observed amplitude of the annual harmonic in 200-mb temperature over Antarctica.

The GCM precipitation is too intense over land, particularly in summer. It is suggested that the problem is related to the parametrizations of moist convection and the boundary layer. The seasonal patterns of precipitation over the western tropical Pacific are generally realistic.

There is no evidence that the GCM systematically underestimates momentum flux convergence.

RÉSUMÉ *Le cycle saisonnier du modèle de circulation générale (MCG) du Goddard Laboratory of Atmospheric Sciences (GLAS) à l'Université du Maryland est analysé en termes du*

comportement des champs moyens mensuels et saisonniers et de la structure de l'harmonique annuelle. (Les tourbillons stationnaires et transitoires sont discutés dans un article complémentaire.)

À haute altitude, la moyenne annuelle des deux régions polaires est beaucoup trop froide, ce qui entraîne des vents zonaux extrêmes au-dessus de 200 mb. Ce problème est plus important pendant l'hiver, mais il est présent en toute saison. On peut trouver une ceinture compensatoire de température plus chaude aux plus basses latitudes. La solution à ce problème ne réside nécessairement pas dans l'inclusion de la traînée des ondes de gravité.

Les harmoniques annuelles simulées de la pression au niveau de la mer et à 200 mb au-dessus de l'hémisphère Nord sont, d'une façon réaliste, intenses au-dessus des continents de l'est et faibles au-dessus des océans de l'est. La simulation est plus difficile en raison des anomalies de la dépression des Aléoutiennes et des basses valeurs des hauteurs au-dessus de l'Europe, ces phénomènes étant hivernaux.

La stimulation des harmoniques annuelles de la pression au niveau de la mer et des hauteurs de la 200 mb est plus réaliste au-dessus de l'hémisphère Sud. LE MCG ne montre pas l'amplitude observée de l'harmonique annuelle de la température à 200 mb au-dessus de l'Antarctique.

La précipitation du MCG est trop intense au-dessus des terres, surtout pendant l'été. Ce problème pourrait dépendre de la paramétrisation de la convection humide et de la couche limite. Les configurations saisonnières de précipitation au-dessus de l'ouest du Pacifique dans les tropiques sont généralement réalistes.

Il n'y a aucune évidence que le MCG sous-estime systématiquement la convergence du flux de quantités de mouvement.

1 Introduction

During the past thirty years, general circulation models (GCMs) have been used for a rich variety of studies aimed at understanding atmospheric motions. Early goals were to accurately simulate the annual or seasonal (usually winter or summer) mean climate, which entailed performing integrations with fixed external boundary conditions. Many of the important features of the atmosphere's general circulation were correctly reproduced, although certain problems were encountered, some of which are still not solved. This success encouraged researchers to use GCMs in sensitivity experiments to study the effects of a variety of boundary conditions and physical processes on the atmosphere's general circulation. These included mountains, clouds, changes in sea surface temperature, soil moisture, albedo, snow cover and sea-ice extent, and changes in the chemical composition of the atmosphere. Since GCMs take into account the non-linear dynamics of the atmosphere as well as the interactions between dynamical processes and the physical processes associated with radiation and moist convection, they have proved useful in providing physical insight into sensitivity problems, even when the time mean climate cannot be simulated perfectly.

More recently, the role of GCMs in the understanding and prediction of climate fluctuations on a variety of time-scales has become more prominent while the quality of the models continues to improve. In addition, the substantial increase in available computing power has made extended (multi-year) simulations fairly popular. It has thus become possible to explicitly model the seasonal cycle of the atmospheric general circulation. The changes in the circulation, temperature and rainfall associ-

ated with the seasonal cycle are larger than any recorded long-term climate change. The seasonal march of solar forcing and the associated change in surface forcing due to the contrasting thermal properties of land and ocean produce large changes in the location and intensity of tropical rain belts and in the amplitude and phase of the extratropical stationary waves, which then modulate the transient fluctuations. In addition, the seasonal cycle interacts with low-frequency atmospheric motions on a variety of time-scales (Straus, 1983). An important example of this is the set of planetary-scale anomalies of the coupled ocean-atmosphere system (El-Niño/Southern Oscillation) that are strongly phase-locked to the seasonal cycle (Rasmusson and Wallace, 1983; Lau, 1985). On a much longer time-scale, the atmospheric response to increases in carbon dioxide is also modulated by the seasonal cycle (Manabe and Stouffer, 1979, 1980; Wetherald and Manabe, 1981). A rather full understanding of the manner in which a GCM handles the seasonal cycle is then seen to be an important prerequisite to the correct interpretation of the GCM's simulation of these non-periodic climate variations. In particular, the accurate prediction of the latter would seem to require a reasonably good simulation of the seasonal cycle.

A number of multi-year integrations (with the seasonal cycle taken into account) have been undertaken recently with moderate-resolution GCMs (horizontal grid spacing of 200 to 400 km, vertical grid spacing of about 100 mb). Manabe and Holloway (1975) studied the seasonal variation of the hydrological cycle in a three-year integration in which the external boundary conditions were prescribed to follow a smooth seasonal cycle. The reported results were limited to quantities of immediate relevance to the hydrological cycle. Mitchell and Bolton (1982) presented the seasonal cycle of total evaporation over land from two versions of the British Meteorological Office GCM, and Manabe et al., (1979) gave the seasonal cycles of some very basic radiative and thermodynamic variables from a coupled atmosphere-ocean model. Randall et al. (1985) presented similar results from a 3-year run of the UCLA GCM, but also included the seasonal cycle of zonally averaged planetary boundary-layer depth.

A more dynamics-oriented discussion was offered by Boer et al. (1984a, 1984b), who reported on the seasonal cycle obtained from a 5-year run of the Canadian Climate Centre's spectral model (triangular truncation T20, hereafter referred to as the CCC GCM). In addition to showing seasonal-zonal means of wind, temperature and humidity, Boer et al. give seasonal mean maps of sea-level pressure, upper-level velocity potential and mid-level temporal standard deviation of height.

Long seasonal-cycle runs have been reported by groups at the Geophysical Fluid Dynamics Laboratory (Manabe and Hahn, 1981; Lau, 1981, 1985) and at the National Center for Atmospheric Research (NCAR) (Chervin, 1986), although very little has been published describing the abilities and limitations of these GCMs in simulating the annual cycle. The NCAR group has reported on perpetual winter and summer runs with the Community Climate Model (CCM), as reported in Pitcher et al. (1983) and Ramanathan et al. (1983). One must exercise care, however, in comparing GCM results from perpetual integrations with those from annual cycle integrations (see Zwiers and Boer, 1987).

An extended (12-year) annual cycle integration was undertaken by the Meteoro-

logical Institute of Japan utilizing a 5-level version of the UCLA GCM. An extensive compilation of seasonal and monthly mean fields is given in a Technical Report (Tokioka et al., 1986). Results from the first January of this integration (Tokioka et al., 1985) and from the first July (Kitoh and Tokioka, 1986) have been published, as well as a detailed description of the simulation of the Asian summer monsoon (Kitoh and Tokioka, 1987) during the first summer. Although the mean circulation and the various components of the mean diabatic heating have been described in some detail in these papers, there is little if any mention of the stationary and transient eddies in mid-latitudes.

Seasonal-cycle integrations with coarser resolution models (either in the horizontal or the vertical or both) have also been carried out. Otto-Bliesner et al., (1982) presented time series of global energetics, global integrals of radiative and nonradiative heating and zonally averaged precipitation from a low-resolution spectral model with 5 levels in the vertical. The seasonal cycle of the net radiation at the top of the atmosphere and the zonally averaged cloud cover, planetary albedo and precipitation in a two-level model were compared by Potter and Gates (1984) with a zonally averaged (statistical-dynamical) model, although only anomalies (i.e. departures from the annual mean) were shown. The structure of the transient eddies in the two-level model was reported in Kushnir and Esbensen (1986a, 1986b), but only for the winter seasons of a multi-year run. Finally, Hansen et al., (1983) compared the seasonal cycle of a number of quantities from two GCMs (with horizontal resolution of order 1000 km) with observations. These authors pay somewhat more attention to dynamical quantities, such as the northward transports of sensible heat and angular momentum, although only in zonally averaged form.

The present series of papers describes the seasonal cycle of the GLAS/U of MD Climate GCM, a model that is currently in use at the University of Maryland (Borger and Vernekar, 1988; Shukla and Fennessy, 1988). This paper discusses the simulation of the seasonal cycle of mean fields and presents the structure of the annual harmonic of selected fields. The second paper in this series (Straus and Shukla, 1988), referred to as SS2, presents the stationary eddies and transient fluctuations for each season, for both the GCM and a variety of observations. The seasonal cycle of energetics is compared with observations by Straus (1988).

The GLAS model has already shown a remarkable degree of success in simulating the monthly and seasonal response of the atmosphere to observed changes in boundary conditions at the earth's surface (Moura and Shukla 1981; Shukla and Wallace, 1983; Fennessy et al., 1985; Shukla and Fennessy, 1988). One of the conclusions of the current paper is that the ability to simulate such relatively short-term climate responses to boundary-condition anomalies does not guarantee a corresponding degree of success in reproducing the seasonal cycle. The GLAS model's simulation of both the annual mean and the seasonal cycle has some significant successes, but also has clear deficiencies. The latter includes excessive zonal winds at upper levels in all seasons (but especially in local winter), and excessive precipitation over land, especially in summer. These errors in the mean forcing and zonally averaged basic state have consequences for the simulation of stationary and transient eddies (discussed in SS2) and for the energy cycle as a whole (Straus, 1988).

The integration presented here uses seasonally varying solar forcing and boundary conditions of sea surface temperature (SST), soil moisture, sea-ice extent, snow and surface albedo. (All boundary conditions are obtained from monthly climatology and are smoothly interpolated in time.) Section 2 presents a brief description of the model and the initial and boundary conditions, and Section 3 describes the method of averaging the observed and model simulated data sets and our general methodology of comparing results. Comparison of the model results with observations are presented in Section 4 for the annual mean and the annual harmonic and in Section 5 for the global fields of monthly and seasonal mean circulation, velocity potential and rainfall. A description of the simulated zonally averaged basic state is given in Section 6. Section 7 gives a summary and discussion.

2 Model description, initial and boundary conditions

a *Model Description*

The model used for this study is a modified version of the GLAS climate model, which has been extensively described in Shukla et al. (1981). The modifications are given by Randall (1982).

The GLAS climate model is global, has nine layers of equal sigma thickness, a 4° latitude by 5° longitude grid, and its upper boundary at 10 mb. The horizontal momentum advection finite-difference scheme conserves momentum and kinetic energy. It also conserves enstrophy in the limit of 2-dimensional nondivergent flow on the equator, and is of second-order accuracy.

The cumulus parametrization scheme is that of Arakawa (1969, 1972), which was developed for the 3-level UCLA GCM but was modified for use in a 9-level model by Somerville et al. (1974). The model includes latent heat release due to large-scale saturation, which occurs when the relative humidity exceeds 100%. Clouds are assumed to occur if and only if the model predicts cumulus convection (restricted to the lowest 6 layers) or large-scale saturation. The vertical diffusion of momentum, sensible heat and moisture above the boundary layer is essentially negligible (coefficient of 0.1 m^2 s^2). A sixteenth-order Shapiro filter is applied once every 30 min to the mass, potential temperature and winds, but only in the longitudinal direction. The long-wave radiation subroutine (Krishnamurthy, 1982) is called once every 5 hours but the heating rates are applied every 30 min, and the short-wave radiation (Davies, 1982) is called every 30 min. A diurnal cycle is included.

The main modifications to the earlier version consisted of changing the parametrizations of the boundary layer, evapotranspiration and cloud-radiation interaction. The boundary-layer parametrization in the new model follows Deardorff (1972), with the assumption that the depth of the planetary boundary layer is 500 m at all grid points and remains constant with time. The surface roughness length is prescribed to be 0.45 m over land, 2.0×10^{-4} m over oceans and 1.0×10^{-4} m over sea-ice grid points. The bulk values of the meteorological fields in the planetary boundary layer are defined at 250 m and are obtained by extrapolation from the two lowest model layers.

The rate of evapotranspiration is, as before, obtained by multiplying beta (β, which is a measure of the prescribed soil moisture) by potential evapotranspiration. Howev-

er, rather than calculating the potential evapotranspiration using the predicted ground temperature (which produces excessive evaporation over land), it is calculated using a saturated lysimeter temperature that is predicted by the model. The functional relationship between β and soil moisture (w) is as suggested by Professor Y. Mintz (pers. commun.): $\beta = 1 - \exp(-6.8w/w^*)$, where w^* is the saturation value of w. This new formulation of evapotranspiration produced notable improvements in evaporation and precipitation over land.

The cloud-radiation interaction was modified by suppressing all clouds from the top 3 model layers. From previous integrations of the GLAS model it was noted that the long-wave cooling associated with the supersaturation clouds in the top layers was one of the primary initiators of excessive cooling at the poles. (It will become apparent that this alteration in cloud-radiation interaction did not solve the "cold-pole" problem). Another alteration in the cloud-radiation interaction was the assumption that cumulus clouds do not interact with short- or long-wave radiation. This is equivalent to assigning a cloud fraction of zero to the cumulus clouds. The assigned cloud fraction was 100% in the previous version, that is, the cumulus clouds were assumed to fill the whole grid box. It was shown by Moeng and Randall (1982) that these changes produced better simulations of solar and long-wave radiative heating for July.

The vertical differencing scheme was also modified for the present model, following Arakawa and Lamb (1977) and Arakawa and Suarez (1982). The modified scheme for the vertical advection of moisture should reduce the problems due to computational moist convective instability. The Fourier filter used to maintain computational stability at the poles was also adapted from Arakawa and Lamb (1977) and is applied only to the zonal wind used to compute the zonal mass flux and to the zonal component of the pressure gradient force.

b *Initial and Boundary Conditions*

The initial conditions were taken from the National Meteorological Center (NMC) analysis of 00 UTC 15 November 1978. Initially, the ground temperature and the surface air temperature are assumed to be equal.

Climatological monthly mean values of SST, soil moisture and surface albedo were prescribed at the lower boundary, and daily values were interpolated using monthly mean values for three consecutive months. The initial value for snow depth is determined empirically from the albedo values, after which the snow depth changes are calculated by model physics. SST fields were obtained from the Geophysical Fluid Dynamics Laboratory (GFDL), and soil moisture fields were taken from Mintz and Serafini (1981). Grid-point values for snow cover were prepared from the corresponding maps produced by the National Oceanic and Atmospheric Administration (NOAA) (Wisenet and Matson, 1976). Surface albedo fields were taken from Posey and Clapp (1964), with some modifications to obtain consistent albedos over all deserts and desert margins. The grid-point values of sea-ice extent for the Northern Hemisphere were prepared from the sea-ice data collected by the British Meteorological Office (1977) and for the Southern Hemisphere from passive microwave satellite observations (Zwally et al., 1983).

3 Data and methods

a *GCM Simulation*

The data used in this study consist of the model output, stored twice per day (at 00 and 12 UTC) and interpolated to pressure surfaces, for the period 1 December 1978 to 30 November 1980, where the significance of the year is only in the time elapsed from that of the initial conditions. The annual harmonic was computed from the twice-daily data, for both the GCM and the observational data sets.

b *Observed Data*

A number of analysis data sets were used in this study as an approximation to the real atmosphere. We loosely refer to these analyses as "observations". For the Northern Hemisphere, we used the NMC operational analyses for the 14½-year period from 1 June 1963 to 31 December 1977, inclusive. The data were obtained from the NCAR data archive, and were available for two times a day (00 and 12 UTC). They were interpolated to a 4° latitude by 5° longitude grid covering the Northern Hemisphere from 22 to 90°N. Temporal linear interpolation was performed to replace missing or obviously erroneous fields. Less than 5% of the data were replaced in this manner.

For the Southern Hemisphere we used several data sets: (i) the European Centre's global analyses of the year of the Global Weather Experiment (GWE), 1 December 1978 to 30 November 1979 (Bengtsson et al., 1982), available twice a day (00 and 12 UTC) and interpolated to a 4° latitude by 5° longitude grid. (ii) 11 years of 500-mb height analyses prepared by the Australian Bureau of Meteorology, from 1 June 1972 to 31 May 1983. A description of the analysis scheme in the early part of the above period is given by Trenberth (1979). The Australian data were obtained from NCAR on a 4° latitude by 5° longitude grid covering the Southern Hemisphere from 90 to 10°S. Only 00-UTC data were used. As with the NMC data, a temporal linear interpolation was performed to replace missing or obviously erroneous fields; less than 5% of the data were replaced.

During the revision stage of these papers we were able to utilize a 7-year set of global European Centre analyses (1980–1986) for some of the observed quantities presented. These data were interpolated to the same 4- by 5-degree grid as before, and were available for two times a day. We refer to these analyses as the ECMWF-7 data set.

For global fields of velocity potential we have used the maps from a recent atlas prepared by Arkin et al. (1986), which is based on a 5-year (1978–1983) average of the operational NMC analyses. For global fields of rainfall we have used data from the atlas prepared by Jaeger (1976). Numerical values of rainfall on a 4° latitude by 5° longitude resolution were obtained from M. Schlesinger of the Oregon State University.

c *Methods of Averaging*

Three sets of time averages were used: the annual mean, four seasonal means and twelve monthly means. The four seasonal means are taken over (i) December, January and February (referred to as DJF), (ii) March, April and May (MAM), (iii) June, July and August (JJA), and (iv) September, October and November (SON).

Any reference to a season (such as winter) in this paper means the season appropriate to the hemisphere under discussion. Time averages were taken over all equivalent periods for each model (or observed) year. Thus, for instance, a DJF mean is the result of averaging the data over each separate DJF in the data set, and then performing a grand mean of the separate means.

d *Interannual Variability and Sampling Error*

When comparing the results obtained from a number of data sets of widely varying record length, as in this paper, estimating the sampling error due to interannual variability is particularly difficult. Ideally one should compare very long GCM simulations with equally long observed data sets in order to minimize the sampling error. (Even in this case, there is the question of how much variability is induced by having different boundary conditions each year in nature.) Clearly the data sets used in this paper fall short of this ideal, and any conclusions reached are subject to the caveat that the sampling errors are not well understood. From the observational standpoint, relying on the GWE year alone is somewhat risky, especially in the Southern Hemisphere, for it is known that the GWE year was characterized by a rather unusual circulation in the Southern Hemisphere (Trenberth, 1984). Further reliance on the 7-year European Centre data set is planned in future work.

4 Annual mean and annual harmonic

a *Annual Mean*

A comparison of the climatological annual mean of the GCM (i.e. the mean over the entire run) with the analyses provides an estimate of the mean bias of the model. Figures 1a and c show the observed annual mean of Northern Hemisphere 500-mb height and 200-mb temperature obtained from the NMC data. The *differences* between the GCM annual mean and the analyses are given in Figs 1b and d. The observed mean 500-mb height shows distinct troughs over the east coasts of North America and Asia, and a weaker trough over Eurasia south of 50°N. Ridges are located in the eastern Atlantic and Pacific oceans, and at high latitudes over Scandinavia. The model bias (Fig. 1b) is generally negative, reaching a peak of about 75 m over Europe, Asia and the eastern Pacific. The major region of positive bias extends from Hudson Bay over the pole to northern Russia. The tendency of the model to overpredict the mid-level height field over northeastern Canada is reflected in the behaviour of the stationary waves, to be discussed in SS2. In the Southern Hemisphere, the model heights (not shown) are consistently less than those of the Australian analyses, with the difference being as large as 150 m polewards of New Zealand. This too is reflected in the model's stationary waves.

The Northern Hemisphere 200-mb temperature field is fairly flat in the annual mean, as shown in Fig. 1c. We show this field to highlight a serious problem of the GCM. As indicated in Fig. 1d, the model is far too cold polewards of 50°N, with a maximum bias near the pole of over 18 K. (The problem is also present in the Southern Hemisphere, where the bias looks remarkably similar to its northern counterpart.) The GCM is also too warm along the latitudinal belt centred at 30°N, the local error being as high as 10 K. In winter, the anomalously warm area extends

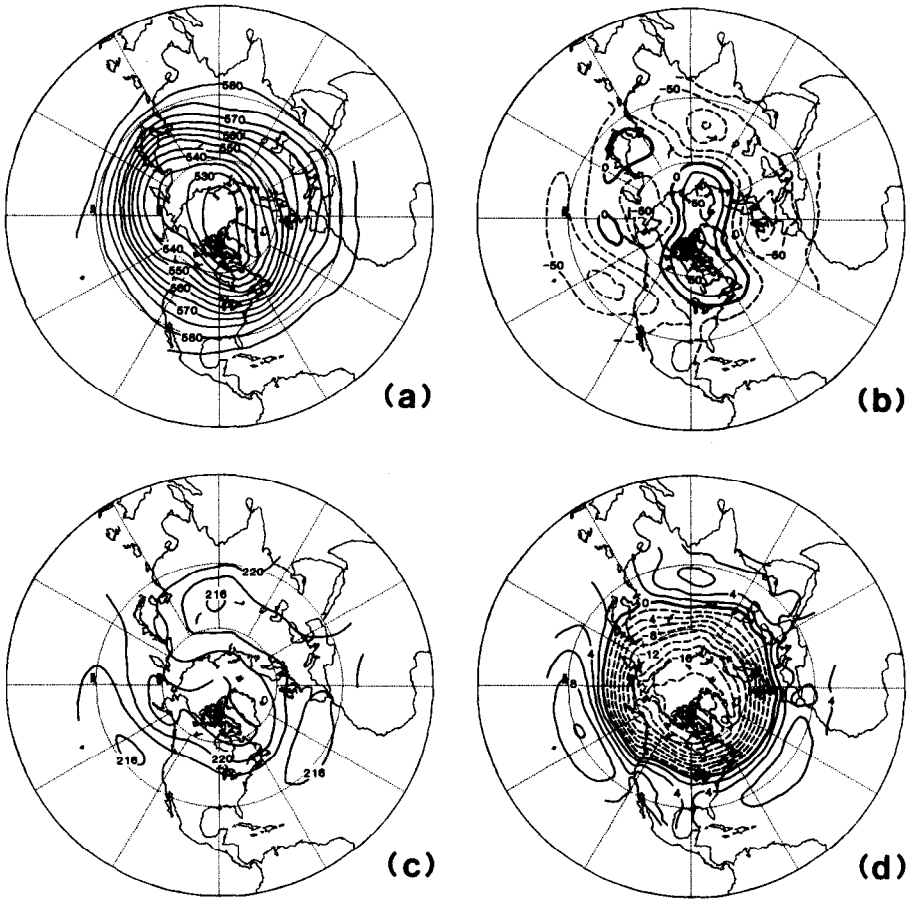

Fig. 1 (a) Annual mean Northern Hemisphere 500-mb height from NMC data, in decametres (contour intervals: 5 dam). (b) Difference between GCM and NMC (GCM minus NMC) annual mean Northern Hemisphere 500-mb heights (contour intervals: [illegible]). (c) Annual mean Northern Hemisphere 200-mb temperature from NMC data (contour interval: 2 K). (d) Difference between GCM and NMC (GCM − NMC) annual mean Northern Hemisphere 200-mb temperatures (contour interval: 2 K).

somewhat farther polewards over the Pacific Ocean. These large biases in the GCM upper-level temperatures will of course be reflected in the upper-level jets (discussed in Section 5), whose structure in turn profoundly affects the stationary and transient waves treated in SS2. We shall return to this problem later in the paper. (The model bias in both 500-mb height and 200-mb temperature look very similar when the seven-year ECMWF global data set is used as a comparison.)

b *Annual Harmonic*

The annual harmonic (or "yearly wave") represents one very fundamental component of the seasonal cycle. The geographical variation of the amplitude and phase of the

annual harmonics of surface quantities has been studied extensively. Hsu and Wallace (1976a, 1976b) presented results for precipitation and sea-level pressure, and White and Wallace (1978) described surface temperature. More recently, Horel (1982) studied the annual harmonics of sea surface temperature, outgoing long-wave radiation and a number of related surface quantities over the tropical Pacific. All these papers contain a number of references to earlier work on the annual harmonics of surface variables. An extensive amount of work on the annual harmonics of both surface and upper-air variables for the Southern Hemisphere has been presented by van Loon (1972a, b), hereafter referred to as vL, and more recently by van Loon and Rodgers (1984a, b). Very little has been published on the annual harmonics of upper-air quantities in the Northern Hemisphere, however, although White and Wallace (1978) present results for the 300-mb height field (amplitude only), and Kousky and Srivatsangam (1983) discuss the temperature and wind fields at several levels over the United States and Mexico.

In this subsection we present the annual harmonics of sea-level pressure, mid-level height and upper-level temperature, as determined from both the GCM and the 7-year set of ECMWF analyses. Figures 2 and 3 present the amplitude and phase of the annual harmonic of sea-level pressure. The contours give the amplitude of the annual harmonic, while the phase is denoted by the direction of the arrows, following the convention of Hsu and Wallace (1976a); southward-pointing arrows denote a 1 January peak in the annual cycle, westward pointing arrows a 1 April peak, northward pointing arrows a 1 July peak and eastward pointing arrows a 1 October peak. We consistently use "maximum" to refer to the *geographical* pattern of *amplitude*, and "peak" to refer to the *temporal* behaviour of the *phase*.

In the Northern Hemisphere, the ECMWF-7 analyses show the continental and oceanic regimes discussed by Hsu and Wallace (1976b). Large amplitudes appear over the Asian continent, with secondary maxima over western North America and the oceans. The continents have peak pressures in winter, whereas the phase of the annual harmonic over the mid-latitude oceans indicates a summertime peak, reflecting the dominance of the Aleutian and Icelandic lows in winter. Also in agreement with Hsu and Wallace (1976b) is the shift in phase in the Arctic, with the peak occurring as late as early April polewards of Scandinavia. In the tropics, the ECMWF data show a summer peak over equatorial Africa, South America, and the Atlantic and western Pacific oceans, with an October peak over the Indian and eastern Pacific Oceans. Over the Pacific basin, the ECMWF results agree well with those of Horel (1982).

The GCM results indicate maximum amplitudes over the Asian continent, with lesser maxima over western North America and the Atlantic, in agreement with the observations. However, the GCM annual harmonic amplitude is unrealistically large in the north-central Pacific near the Gulf of Alaska. This occurs because the GCM sea-level pressure is consistently too low during winter in this region, and is somewhat too high for most of the rest of the year. The overestimate of the winter Aleutian low in the GCM is similar to the problem that occurs in many high-resolution GCMs when gravity wave drag is omitted (Palmer et al., 1986).

Whereas the phase of the GCM annual harmonic over Asia and western North America correctly indicates a January peak, the harmonic peaks in the mid-latitude

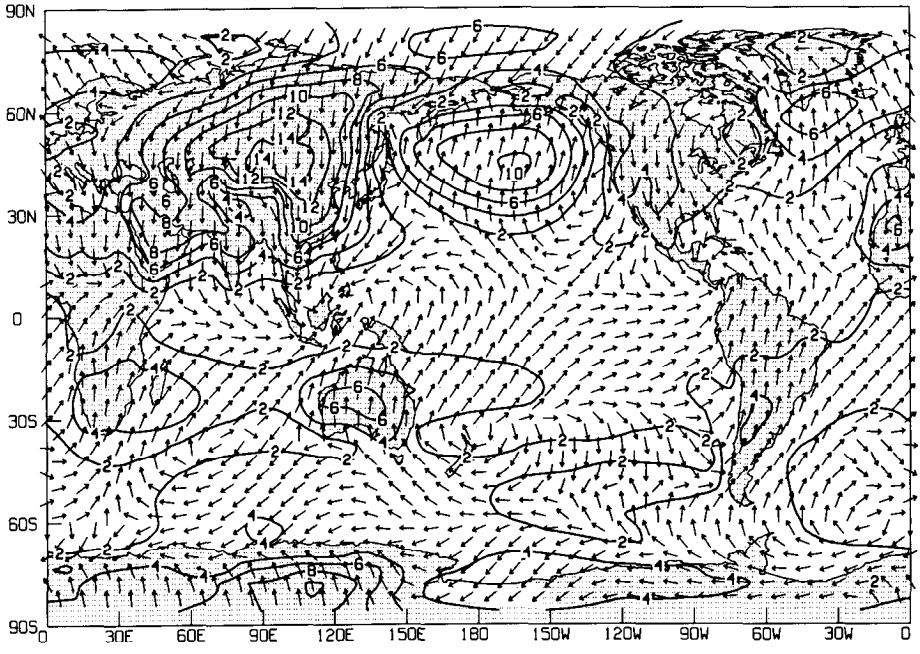

Fig. 2 Amplitude and phase of the annual harmonic of sea-level pressure from ECMWF-7 data (contour interval: 2 mb). See text for further explanation.

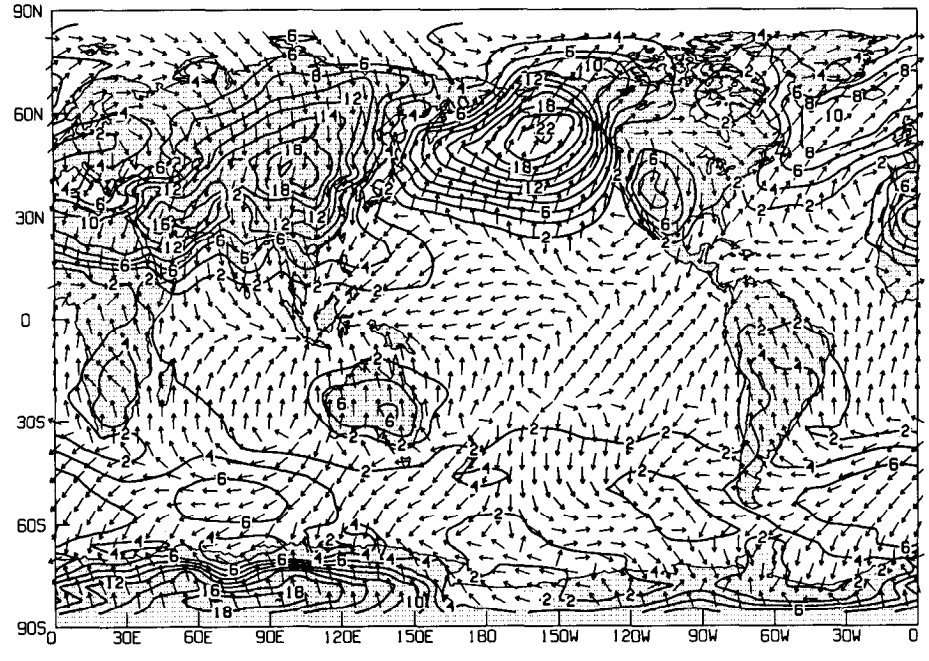

Fig. 3 Amplitude and phase of the annual harmonic of sea-level pressure from the GCM (contour interval: 2 mb).

Atlantic and Pacific occur a month or so later than that observed. In addition, the simulated harmonic over Canada and most of the Arctic is generally out-of-phase with the observations.

The simulated phases over equatorial Africa, South America and the eastern Pacific correctly imply a summer peak, and those over the Indian Ocean a fall peak. Both the analyses and the GCM indicate a sharp transition in the phase of sea-level pressure from the eastern tropical Pacific to the western tropical Pacific. However, the GCM phases peak consistently several months too early in this region.

In the Southern Hemisphere the ECMWF-7 results and those of Hsu and Wallace (1976b) and vL give maximum amplitudes over the subtropical land masses of South Africa, South America and Australia, with peak values occurring during July. These data sources further agree that the South African maximum extends eastward into the Indian Ocean. The GCM results also generally indicate large values of the amplitude over land with midwinter peaks, although the phase over South Africa leads that of the observations.

The GCM amplitudes (Fig. 3) in the mid-latitude Indian and Pacific oceans generally resemble the ECMWF-7 results, but the large simulated maximum in amplitude in the South Atlantic is somewhat exaggerated. The observed winter/spring peaks in phase in the subtropical oceans and the basic pattern of summer/fall peaks in the Pacific and Indian mid-latitude oceans are evident in the GCM results. However, the simulated peaks in phase during summer/fall in the South Atlantic are anomalous.

The amplitude of the annual harmonic of the 500-mb height field from the ECMWF-7 data set (Fig. 4) is in excess of 200 m over the northeast portions of the Asian and North American continents, with the largest values occurring over the east Asian coast and in north-central Canada. Minima are apparent in the eastern oceans, and the amplitudes rapidly decrease as one approaches the subtropics. The phases indicate a late summertime peak, with little change between the high-latitude oceans and continents and a more discernible lag in the mid-latitude oceans. The ECMWF GWE results (not shown) yield substantially the same pattern. The GCM (Fig. 5) reproduces the maximum in amplitude over the east coast of Asia and the plateau over northeastern North America, although the former is considerably stronger than what is observed. The anomalous GCM centre over the Gulf of Alaska results largely from the poor simulation of the seasonal cycle of sea-level pressure; the monthly mean 500-mb heights follow the same pattern (low in winter, high in summer) as the sea-level pressure. The overly strong GCM Asian maximum is due more to problems with simulating the lower tropospheric temperatures than to problems with the sea-level pressure. Note that the observed minima in amplitude over the eastern oceans are well simulated, except for an eastward shift of the eastern Pacific minimum by about 15° of longitude. The maximum over north-central Canada is also captured by the GCM. The simulated phases are approximately correct, but show less ocean-continent lag than what is observed.

The ECMWF-7 data yield a very broad maximum in annual harmonic amplitude over the Indian and Pacific oceans, with a broad minimum polewards of this (Fig. 4). In addition, quite localized maxima are seen in the Atlantic at 40°S and over the Antarctic coast near the date-line. Note that the values of the annual harmonic amplitude are much lower than in the Northern Hemisphere. The annual harmonic

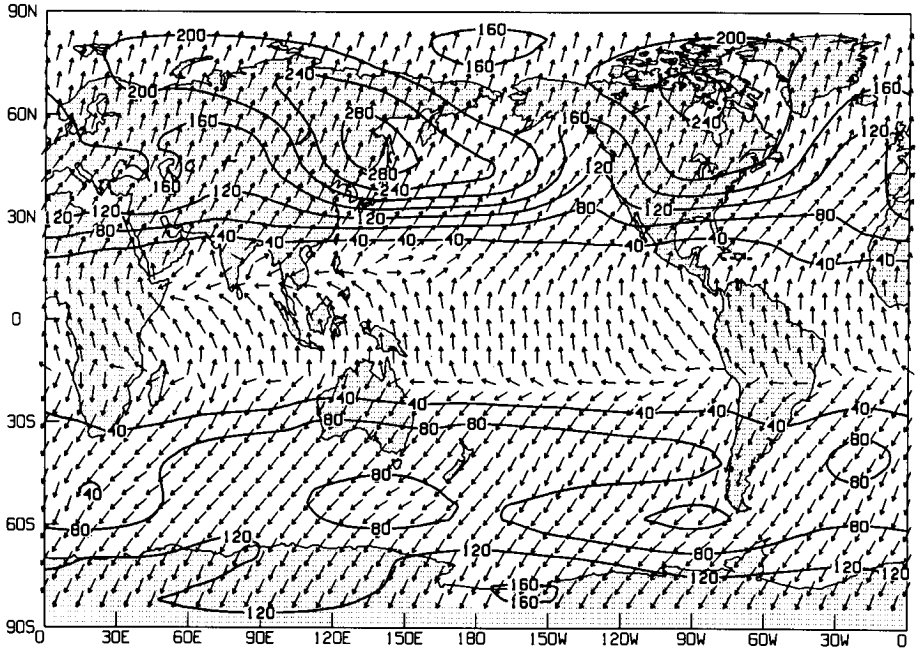

Fig. 4 Amplitude and phase of the annual harmonic of 500-mb height from ECMWF-7 data (see text for further explanation). Contour interval: 40 m.

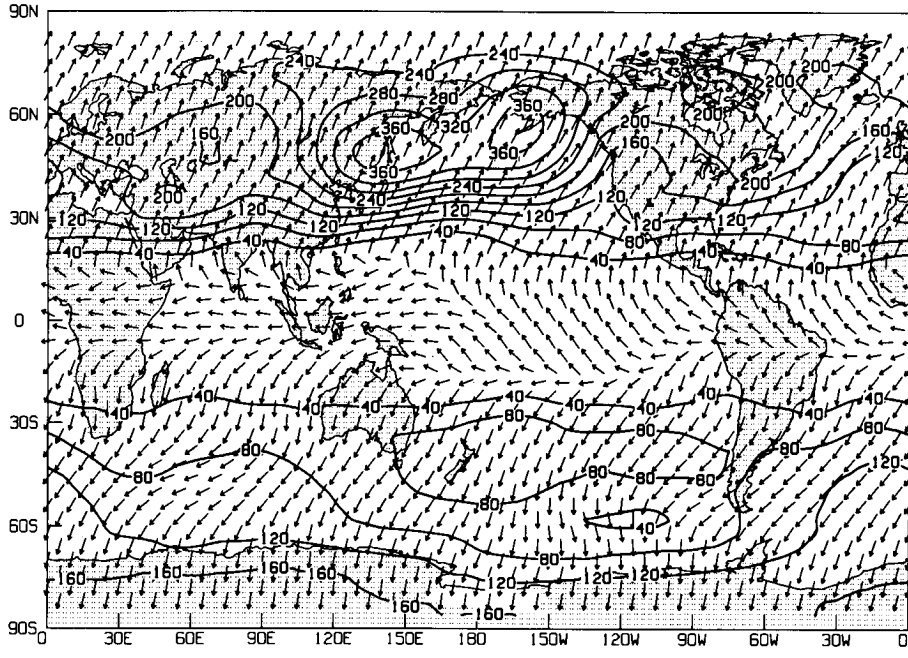

Fig. 5 Amplitude and phase of the annual harmonic of 500-mb height from the GCM (see text for further explanation). Contour interval: 40 m.

peaks in late summer over most of the hemisphere, whereas polewards of South Africa and the Australian–New Zealand region the phases indicate an early autumn peak. (The structure of the annual harmonic given in Fig. 4 is in good agreement with that of vL and generally agrees with the structure yielded by the ECMWF GWE data.)

The GCM captures the broad maximum in annual harmonic in the South Pacific, and also reproduces the minimum polewards of 50°S in the Pacific. The simulated annual harmonic amplitudes over Antarctica are somewhat too high west of the date-line. The GCM phases are realistic in a broad sense, indicating a peak in the annual harmonic in late summer at most locations and in early autumn in the mid-latitude Indian Ocean.

The observed annual harmonic of 200-mb height in the Northern Hemisphere (not shown) is nearly the same as at 500 mb, except that the amplitudes are larger. The anomalously large amplitude of the GCM annual harmonic over east Asia is quite evident at 200 mb, but the anomalous GCM centre over the Gulf of Alaska is much less prominent than at lower levels. Minima continue to appear over the eastern oceans, although they are not as pronounced in the GCM results as they are observed to be. Over Europe, the simulated amplitudes are far too large, a result of the GCM's winter heights being far too low (over 300 m in the monthly mean) in this region. (A similar problem is noted in the Community Climate Model (CCM) of NCAR for perpetual January simulations (Pitcher et al., 1983), although it is not as severe as in our results.) Over the tropical Pacific there is again a sharp transition in the phase of the annual harmonic from the ECMWF-7 data, with summertime peaks in the eastern Pacific giving way to spring peaks in the western Pacific and Indian oceans. This transition is conspicuously absent in the GCM.

Figure 6 shows the observed annual harmonic of 200-mb temperature. Over the Northern Hemisphere, it has a sizable amplitude only over the east Asian continent and polewards of 60°N. The GCM, in contrast, shows strong values of the amplitude throughout mid-latitudes with maximum values of 16 K over Europe and an additional local maximum of 8 K over the central Pacific near 40°N (Fig. 7), the latter corresponding to an observed minimum. This unrealistic behaviour results because the simulated winter temperatures are far too warm over the northern mid-latitude oceans (up to 20 K too warm in the Pacific), and are far too cold over Europe, Asia and North America, a reflection of the "cold pole" problem suffered by the GCM. Poleward of 50°N, the simulated phases indicate an August peak, one month later than what is observed.

The pattern of annual harmonic amplitude in the observed temperature at 200 mb is quite zonal in the Southern Hemisphere, with values increasing rapidly polewards of about 45°S. (At 300 mb this rapid increase is not seen.) Whereas the GCM shows some mid-latitude gradient of the annual harmonic in the Southern Hemisphere, the amplitude does not change much polewards of 60°S, so that the simulated amplitude over Antarctica is too weak.

5 Monthly and seasonal means

a *Zonally Averaged 200-mb* u-*Wind*

The seasonal variation of the strength and position of the zonally averaged 200-mb jet stream is portrayed in the form of latitude/time sections of the zonal wind for the GWE

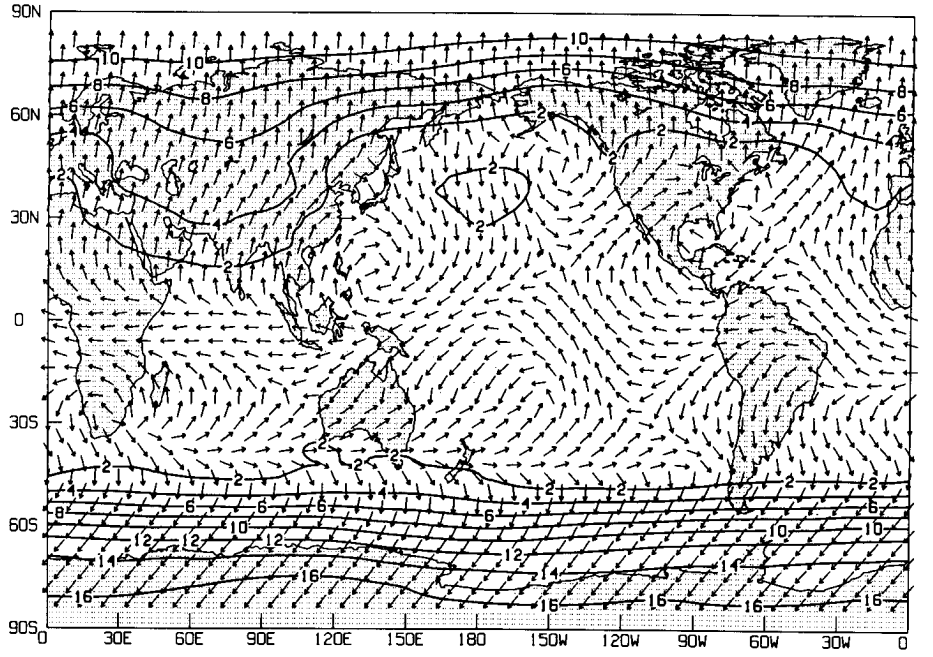

Fig. 6 Amplitude and phase of the annual harmonic of 200-mb temperature from ECMWF-7 data (see text for further explanation). Contour interval: 2 K.

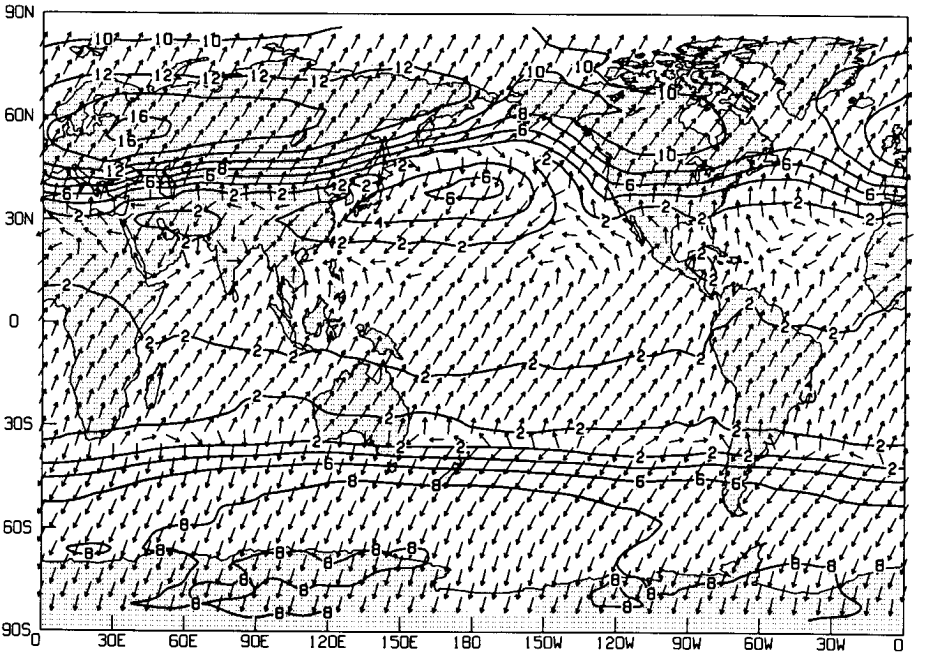

Fig. 7 Amplitude and phase of the annual harmonic of 200-mb temperature from the GCM. Contour interval: 2 K.

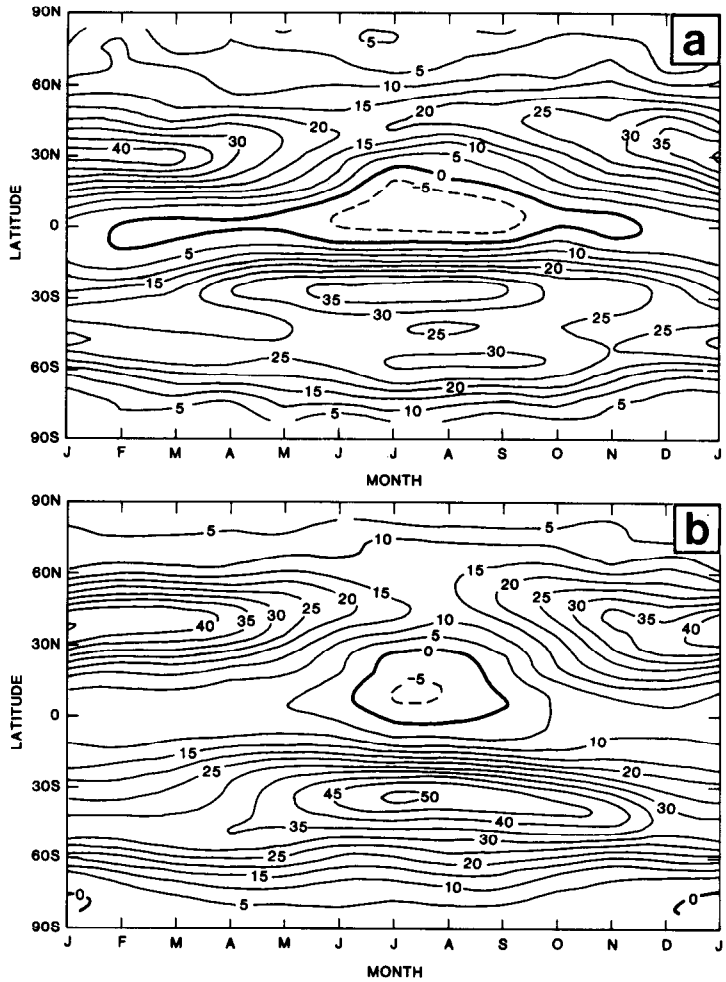

Fig. 8 Latitude/time sections of zonally averaged 200-mb u-wind, based on monthly means (a) from the ECMWF GWE data and (b) from the GCM. Contour interval: 5 m s^{-1}.

analyses (ECMWF) and the GCM in Fig. 8. In the Northern Hemisphere, the zonally averaged GCM jet has the correct magnitude in (northern) winter, but is located too far polewards. This is primarily due to the model's placement of the east Asian jet 5 to 10° northward of the observed position for the GWE year.

During the southern winter (JJA), the model's zonally averaged subtropical jet in the Southern Hemisphere is about 50 m s^{-1}, much stronger than observed during the GWE, and is also located too far polewards. The secondary maximum in the u-wind seen in the GWE data has no counterpart in the simulation, and its occurrence in the zonal mean was thought to be one of the unusual aspects of the GWE year (Trenberth, 1984). However, more recent studies utilizing ECMWF's analyses for 1979–1982 have confirmed this feature (Trenberth, 1987). In the southern winter, the field of the

u-wind in the GCM has the observed magnitude over Australia (where the observations show the u-wind to peak), but at most other longitudes the GCM u-wind field is much too strong. The result is a nearly uniform circumpolar jet in the simulated Southern Hemisphere winter.

b *Velocity Potential and Rainfall*

Figures 9 and 10 show the observed (NMC) and simulated seasonal maps of 200-mb velocity potential, and Figs 11 and 12 show the seasonal maps of precipitation. (The reader should recall that an additive constant does not change the interpretation of the velocity potential.)

The large-scale minimum in the Pacific Ocean in winter (DJF), which corresponds to upper-level divergent flow, shifts northward in spring while it weakens, and then shifts both northwards and westwards in summer while it strengthens.

The simulated velocity potential also shows a strong region of upper-level divergence over the Pacific Ocean throughout the year. The gradients are consistently stronger than observed, the discrepancy being the greatest in the northern fall (SON). Furthermore, the modelled seasonal shifts in the position of the minimum, even though in the right direction for each seasonal transition, are not large enough. This is particularly evident in summer, where the GCM minimum is located too far south and east, much closer to the spring and fall positions than observed. Thus the GCM upper-level divergence maximum in the Pacific clings to the equator, just westward of the date-line, whereas in the observations this maximum exhibits a more seasonal movement.

The simulated Atlantic velocity potential compares well with the NMC observations in regard to overall positioning and strength of gradient, but the same cannot be said for the velocity potential over Africa and the Indian Ocean. Whereas the observations show upper-level convergence in all seasons in these regions, (with the exception of sub-Saharan Africa during summer (JJA)), the GCM flow field indicates upper-level divergence in the northern winter (DJF), spring (MAM) and fall (SON).

Turning to the seasonal maps of rainfall, we attempt to correlate the patterns of velocity potential with those of rainfall maxima, which are, of course, of much smaller scale. The observed velocity potential minimum over the Pacific basin is clearly associated with the rainfall maximum of over 8 mm d^{-1} in the central Pacific, Indonesia and (in JJA) in India. Furthermore, the northward and westward shift of upper-level divergence in going from spring (MAM) to summer (JJA) is associated with corresponding shifts in rainfall. (A possible inconsistency between the independent observational data sets of rainfall and velocity potential is noted over South America, where during DJF and MAM, the rainfall maxima of over 8 mm d^{-1} correspond to only very weak upper-level divergence.)

The GCM rainfall correctly shows a maximum in the Central Pacific/Indonesian region in all seasons, but the magnitude of the rainfall (over 16 mm d^{-1}) is far too large, corresponding to the GCM's excessive upper-level divergence in this region. The "centre-of-mass" of the Pacific rainfall pattern remains closer to the equator (i.e. it shifts less with season) than what is observed, a problem that was already noted in the behaviour of the velocity potential. However, the accuracy of the observed

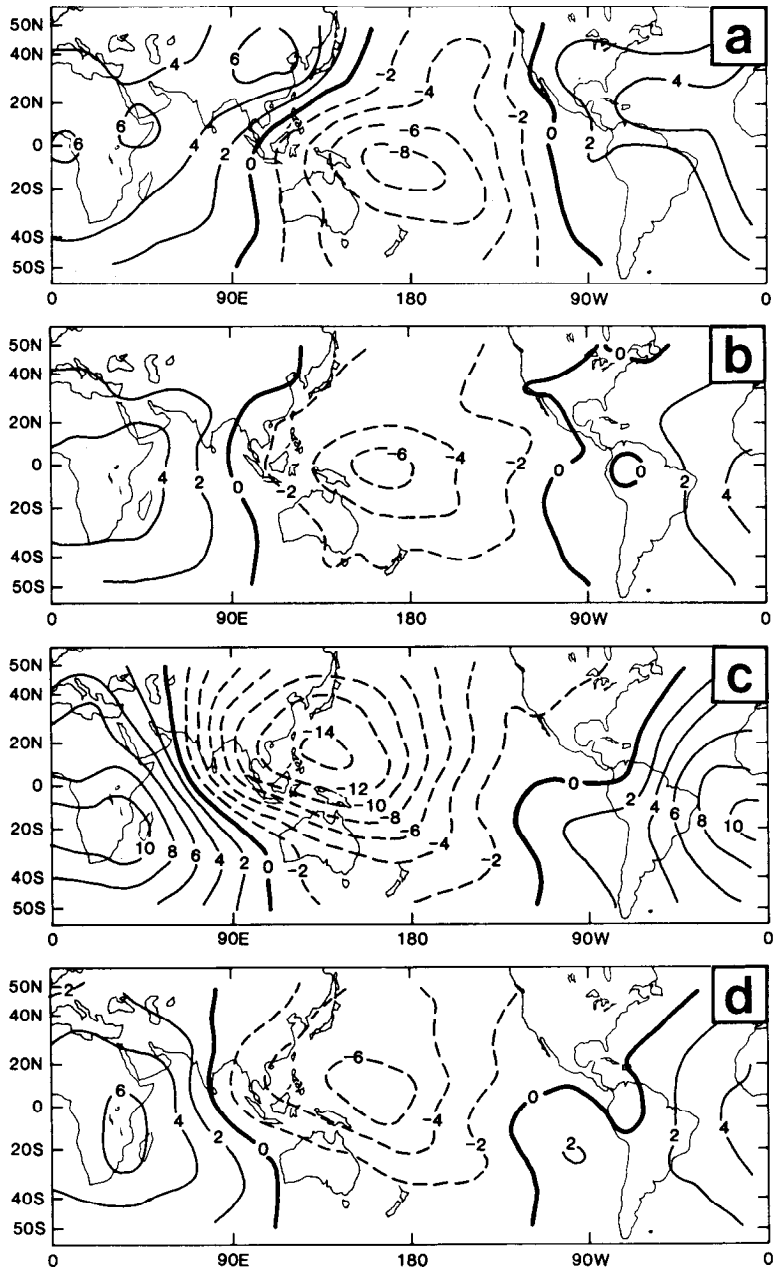

Fig. 9 Seasonal mean 200-mb velocity potential, from Arkin et al. (1986). Contour interval: 2×10^6 m^2 s^{-1}. (a) DJF, (b) MAM, (c) JJA and (d) SON.

rainfall amounts over the oceans is not known. We thus do not have sufficient confidence in the observed oceanic amounts to give a quantitative estimate of the error in the model-simulated rainfall. Based on an examination of the seasonal mean outgoing long-wave radiation, it is our impression that the seasonal persistence of the

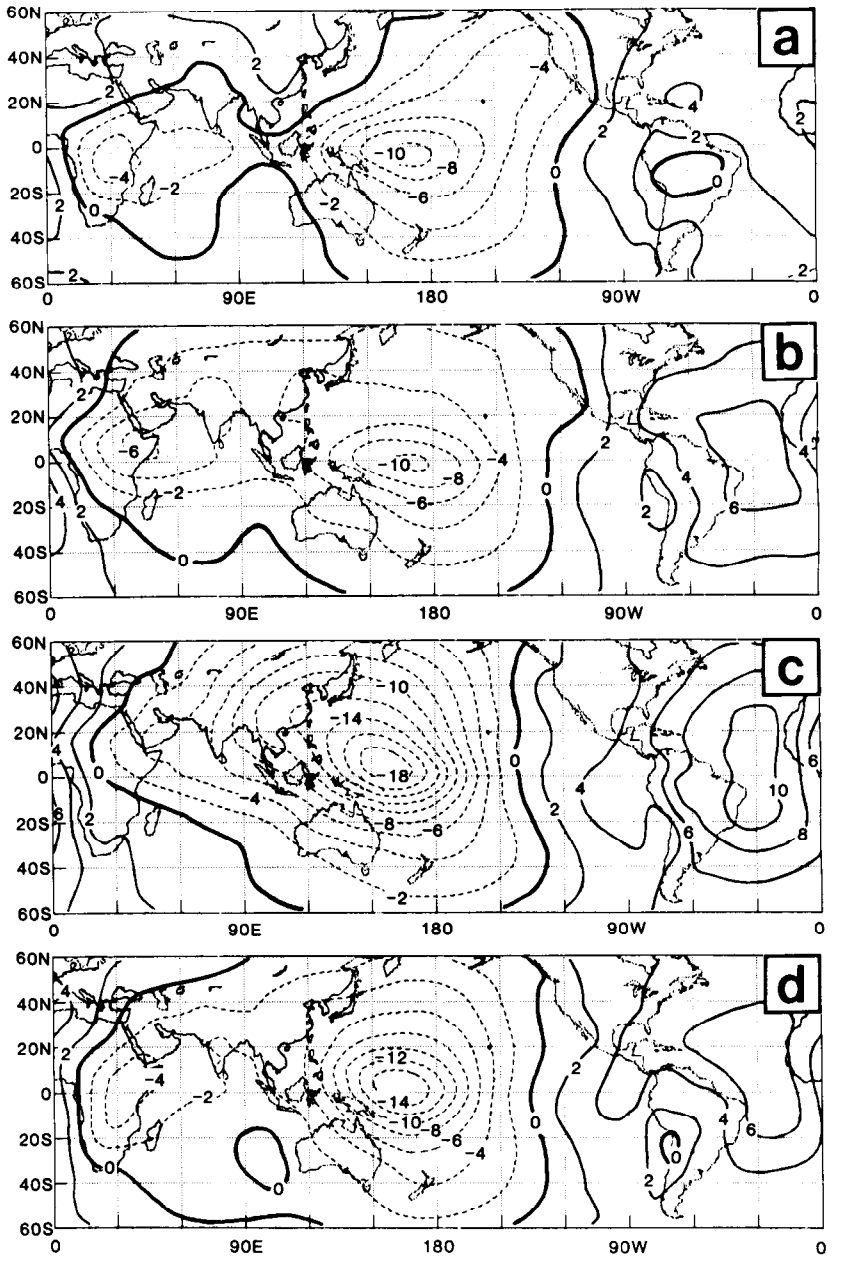

Fig. 10 Seasonal mean 200-mb velocity potential, from the GCM. Contour interval: 2×10^6 m^2 s^{-1}. (a) DJF, (b) MAM, (c) JJA and (d) SON.

equatorial rainfall maximum over the western Pacific is *not* well captured by the observations of Jaeger (1976).

Turning to the modelled rainfall over land, we see that the most conspicuous discrepancy in winter (DJF) is the excessive precipitation over Africa in the region

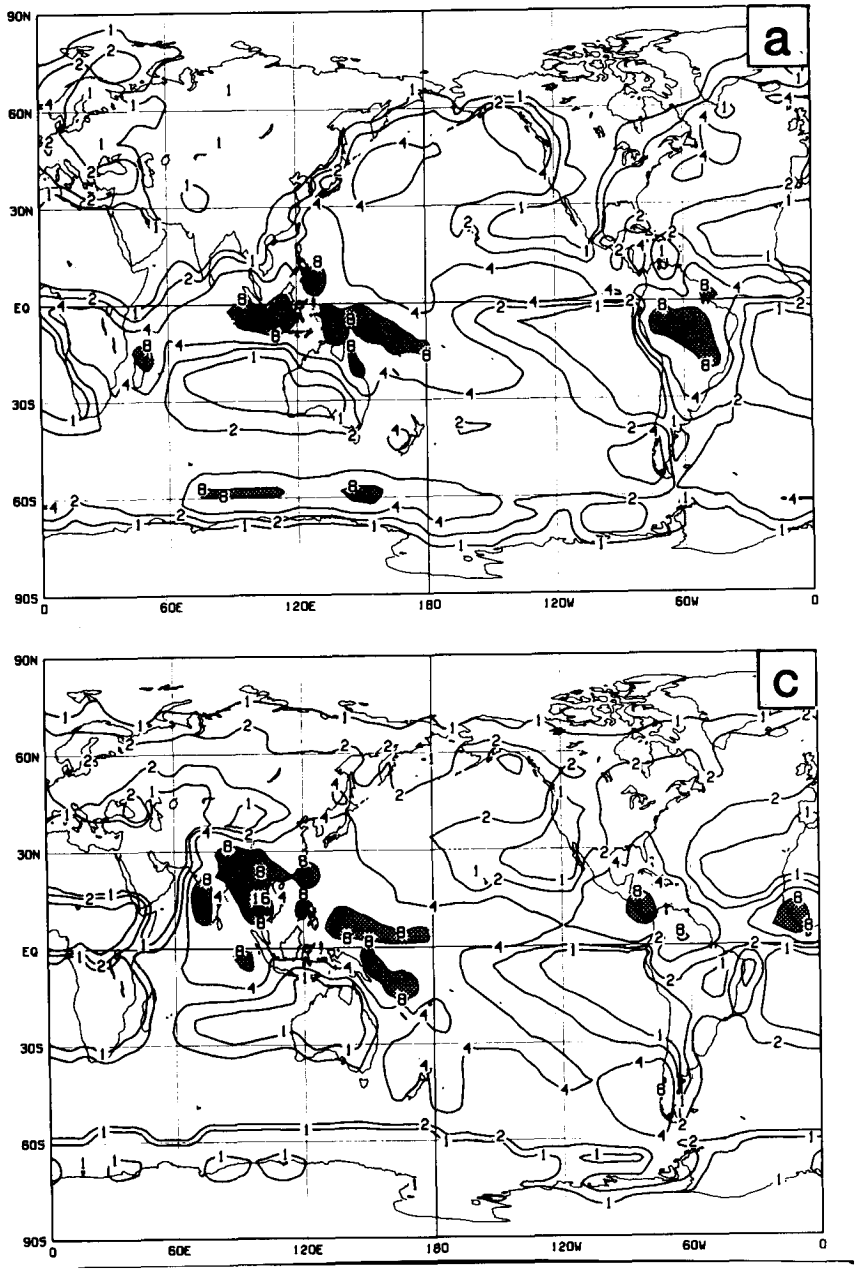

Fig. 11 Seasonal mean observed rainfall, from Jaeger (1976). Contours are drawn for 1, 2, 4, 8 and 16 mm d^{-1}. (a) DJF, (b) MAM, (c) JJA and (d) SON. Light shading denotes values between 8 and 16 mm d^{-1}, dark shading values over 16 mm d^{-1}.

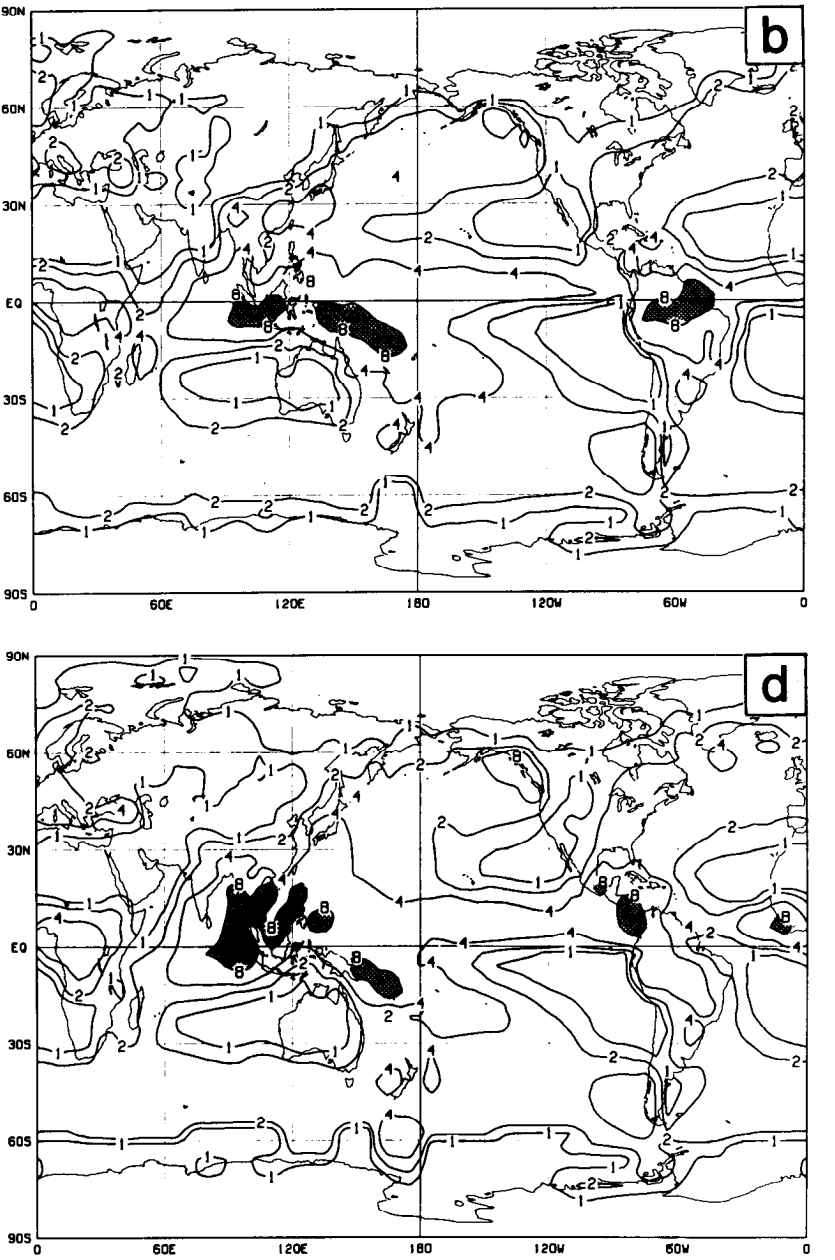

Fig. 11 (*Concluded*).

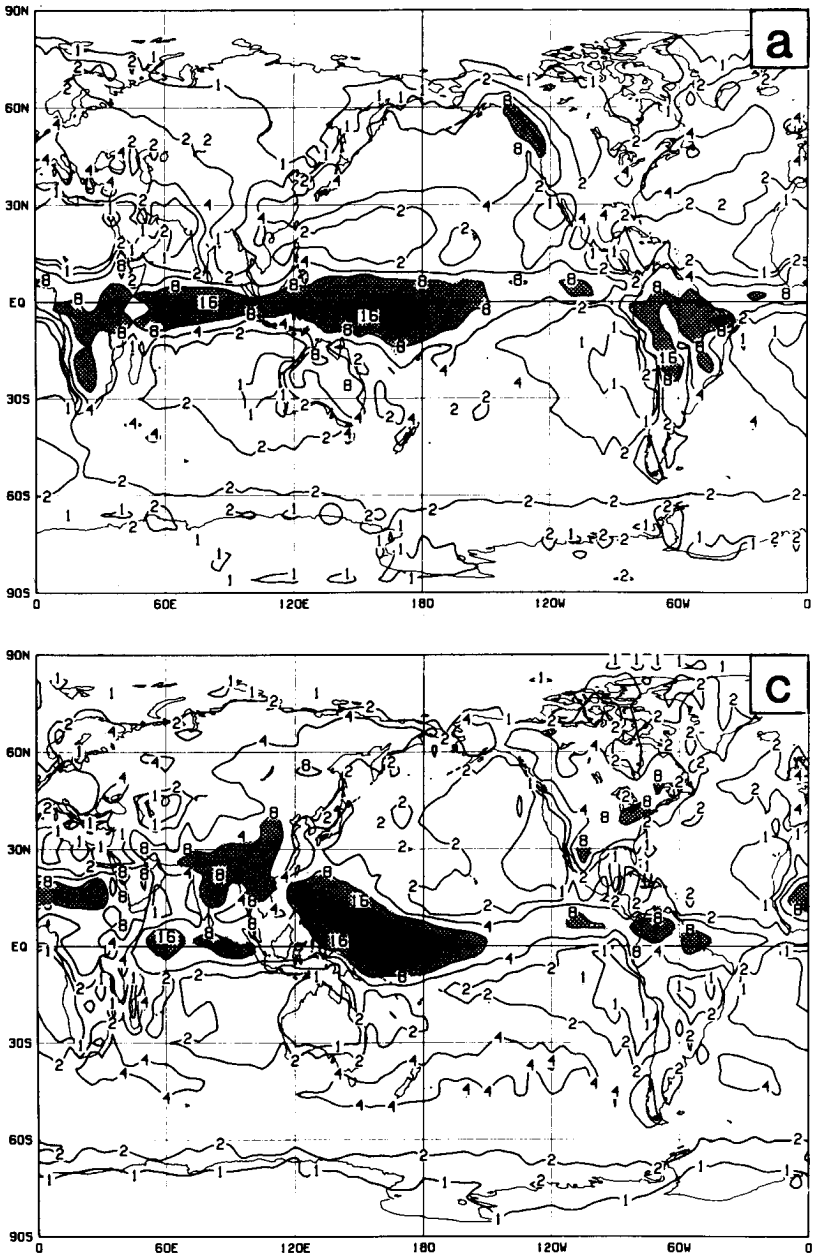

Fig. 12 Seasonal mean GCM rainfall. Contours are drawn for 1, 2, 4, 8 and 16 mm d^{-1}. (a) DJF, (b) MAM, (c) JJA and (d) SON. Light shading denotes values between 8 and 16 mm d^{-1}, dark shading values over 16 mm d^{-1}.

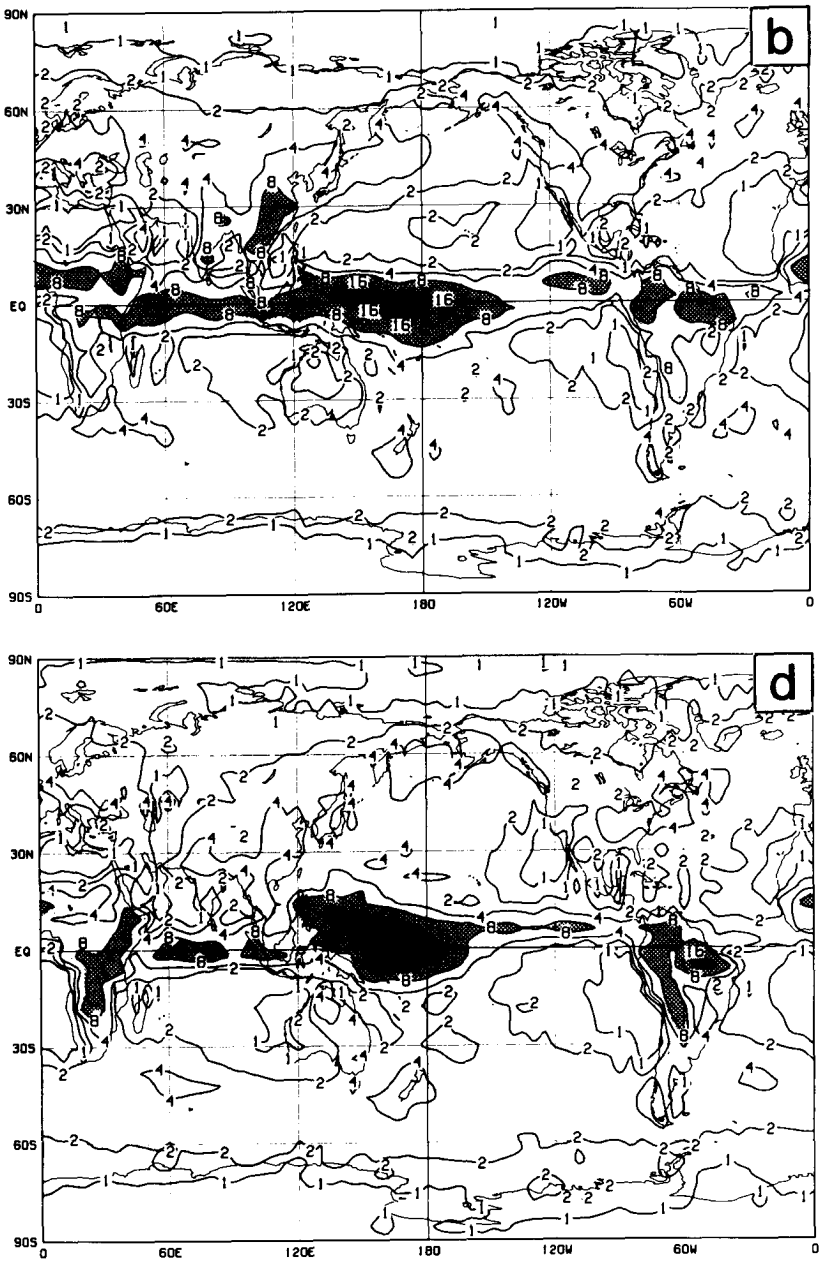

Fig. 12 (*Concluded*).

lying between the equator and 20°S. In fact, the precipitation averaged over land between the equator and 20°S is nearly twice as large as that observed. In contrast, the simulated rainfall over South America is quite realistic. Although the pattern of GCM rainfall over North America, Europe and Asia is realistic the magnitude is consistently too high.

A subsequent anomaly in precipitation appears just south of the Sahara in the GCM during spring, and it intensifies as it moves northward in summer to the point where the model produces excessive rainfall over the Sahara desert. The simulated rainfall over North America is also excessive in spring and summer. The anomaly in subtropical South Africa (having weakened in MAM and JJA) is again quite prominent in the fall (SON), when it is accompanied by a similar anomaly in subtropical South America.

Studies with a GCM very similar to the one considered here (Sud and Molod, 1987) have suggested that the GCM's excess precipitation in summer in general, and over the Sahara desert in JJA in particular, are due to the absence of sufficient vertical mixing of moisture near the ground. This leads to the accumulation of moisture appearing in low levels from large-scale convergence, and hence eventually to spurious rainfall. Further study of the GCM's parametrizations of moist convection and the boundary layer is needed to solve this problem. We should point out that the GLAS/UMD Climate GCM does have a diurnal cycle in incoming solar radiation.

It is quite significant that other GCMs share many of the problems in the simulation of precipitation seen in the GLAS GCM. The persistence of very substantial precipitation near the equator in the Pacific noted in the GLAS GCM is also apparent in results from the CCC GCM (Boer et al., 1984b). Both the CCC GCM and the climate GCMs of Hansen et al. (1983) also yield excessive precipitation over Africa south of the Equator in DJF. While NCAR's CCM does not show this particular error, its rainfall amount in the northern winter, averaged between the equator and 20°S, is similar to what we report for the GLAS GCM and is thus too large (see Fig. 8 of Pitcher et al., 1983).

With regard to precipitation over land, the GCMs reported by Hansen et al. (1983) give excessive summertime rain over the southern edge of the Sahara, although the problem may not be as severe as in our case. Both the CCC GCM and NCAR's CCM show too much rain over North America in summer, and the anomaly over South America that we report for the southern spring is also seen in the CCC GCM. This preliminary comparison of rainfall in various GCMs indicates a good deal of overlap in problem areas. Whether this is due to some common design inadequacy in these widely different models remains an open question.

6 Zonally Averaged basic state

In order to aid in the interpretation of the simulated stationary waves and transient fluctuations (to be discussed in SS2) it is helpful to have the zonally averaged basic state available. Figure 13 shows seasonal mean latitude/height sections of the zonally averaged u-wind (solid lines) and temperature (dashed lines) from the ECMWF GWE data, and Fig. 14 gives the corresponding GCM results.

The excessively low, polar temperatures that plague the GCM are reflected in the

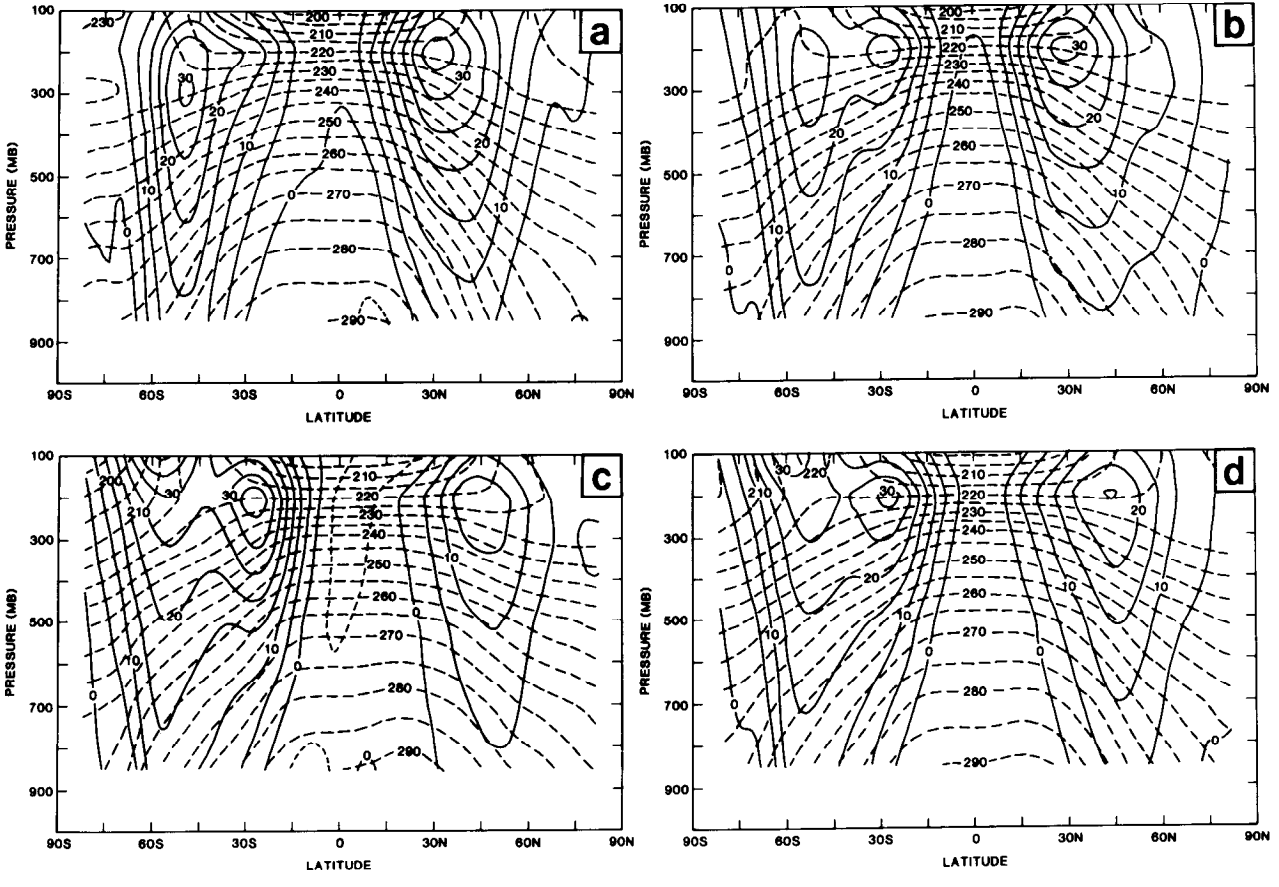

Fig. 13 Seasonal mean latitude/height sections of zonally averaged u-wind (solid lines) and temperature (dashed lines) from the ECMWF GWE data. Negative u-winds (easterlies) are indicated by short dashes. Contour interval: 5 m s^{-1} for u-wind, 5 K for temperature. (a) DJF, (b) MAM, (c) JJA and (d) SON.

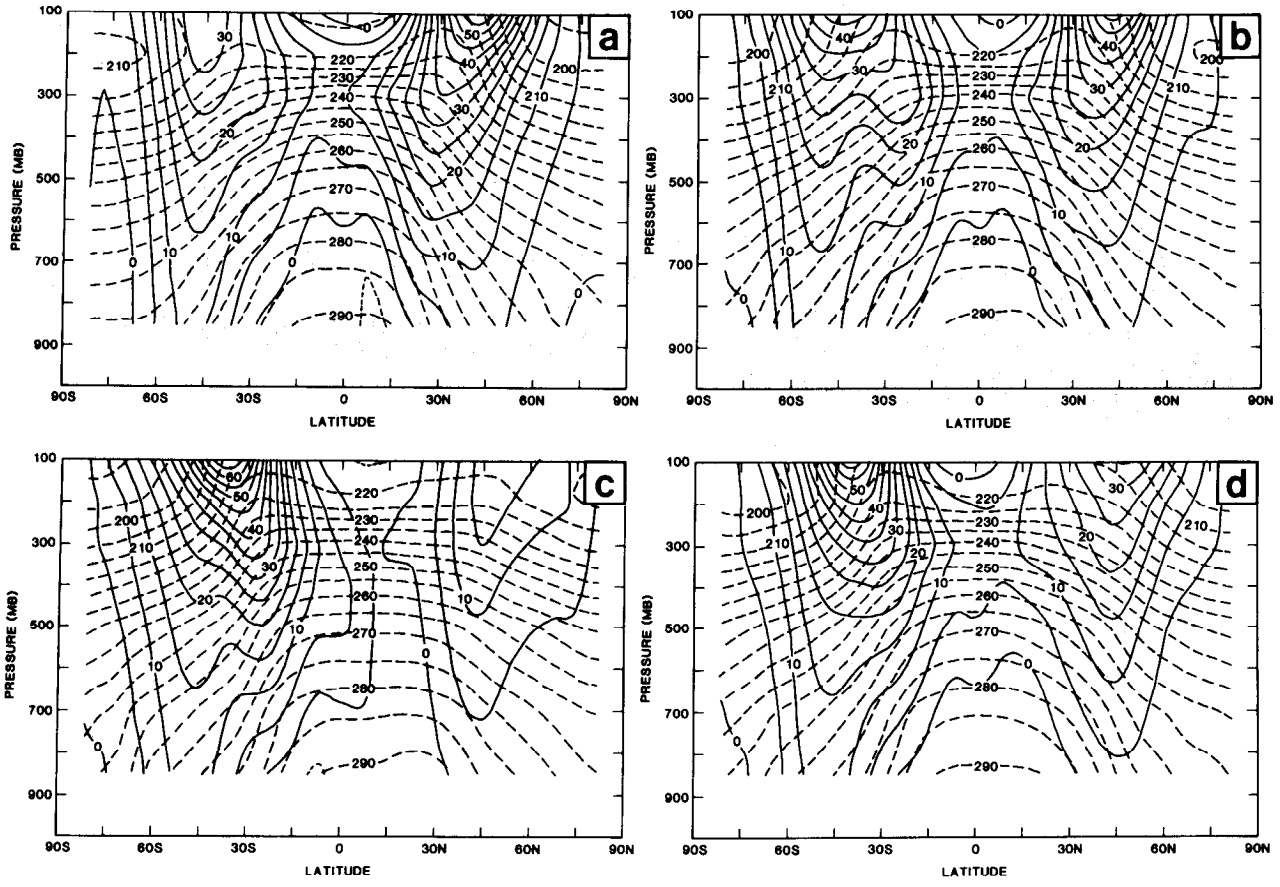

Fig. 14 As Fig. 13, except for the GCM. Negative u-winds (easterlies) are indicated by short dashes. Contour interval: 5 m s^{-1} for u-wind, 5 K for temperature. (a) DJF, (b) MAM, (c) JJA and (d) SON.

failure of the zonally averaged u-wind to decrease with height in the upper troposphere as it is observed to do. This problem is greater in winter than in summer, but it is present throughout the year. Thus the simulated winter jets (DJF in the Northern Hemisphere, JJA in the Southern Hemisphere) are stronger than observed above 300 mb, the discrepancy being greatest at 100 mb (the top level displayed), whereas in the southern summer the simulated jet is actually too weak below 200 mb. In the MAM average, the GCM jets in both hemispheres are very similar and are only slightly weaker than the Northern Hemisphere DJF average, leading to simulated winds considerably in excess of those observed at 100 mb. A much greater degree of interhemispheric asymmetry in the simulated results is present in SON, for now the jets strongly resemble their JJA configurations. The downward penetration of the polar night (stratospheric) jet into the troposphere in the southern winter and spring is not reproduced by the GCM. A hint of the observed double-jet structure is apparent in the simulated MAM results, however. In the lower troposphere, it is noteworthy that the GCM's Southern Hemisphere mean zonal wind (and its vertical shear) are consistently too small.

7 Summary and discussion

a *Summary*

The annual mean 500-mb heights show a relatively modest bias (maximum of 75 m) in the Northern Hemisphere but a larger bias (as much as 150 m) in the Southern Hemisphere.

Both polar regions at upper levels are much too cold (~20 K) in the annual mean. This "cold pole" error is also reflected in the unrealistically large magnitudes of the upper-level zonal winds. The problem is present in all seasons but is particularly severe in local winter. There is a compensating warm belt in the subtropics and low mid-latitudes.

In the lower troposphere, the GCM's Southern Hemisphere mean zonal winds (and their vertical shear) are consistently too weak.

The GCM rainfall and velocity potential show the observed maximum in precipitation (and upper-level divergence) in the Pacific (near the date-line) throughout the year, although the GCM rainfall is too strong (divergence too large).

There is generally too much precipitation over land. The problem is most noteworthy in summer, when the GCM simulates rainfall over the Sahara desert and anomalies over North America, Europe and Asia. The problem can be partially traced to the parametrizations of moist convection and the boundary layer, and in particular to inadequate vertical mixing of moisture at low levels.

The simulated annual harmonic of the Northern Hemisphere sea-level pressure and upper-level height captures the observed tendency to have a strong harmonic over the eastern continents and a weak one over the eastern oceans.

Significant deviations between the simulated and observed harmonics for the sea-level pressure and upper-level heights in the Northern Hemisphere are manifestations of:

- The anomalously deep Aleutian low in winter
- The very low values of the geopotential height predicted during winter over Europe

The GCM mid-level temperature annual harmonic is generally realistic, but at upper levels it is too large, owing to the simulated upper-level winter temperature being far too cold over continents (the "cold pole") and too warm over oceans.

In the Southern Hemisphere, the GCM's sea-level pressure annual harmonic is fairly realistic. The observed 500-mb patterns of maximum amplitude for temperature and height near New Zealand and the minimum poleward of this are present in the GCM results.

At upper levels the GCM fails to show the observed dramatic increase of the annual harmonic in temperature near Antarctica.

b *Discussion*

Clearly one of the most deficient features of the simulation is the extensive cooling in the upper troposphere near both poles and the compensating warming over lower latitudes, both being associated with upper-level zonal winds that are much too strong. Since the model-simulated vertical wind shear above 200 mb is opposite in sign to that observed, it is likely that the wave propagation and reflection properties of the model's basic zonally averaged state are not completely realistic. In fact, in SS2 we find distinct errors in the stationary and transient wave variances at upper levels.

The lack of negative shear above the 200-mb jets is found in many GCMs (Tenenbaum, 1982). Boer et al. (1984a, b) find that introducing a gravity wave drag parametrization into the relatively low-resolution (T20) CCC GCM ameliorates this problem but by no means solves it. This type of parametrization takes into account the momentum transfer in the vertical of (unresolved) orographically generated gravity waves that may break in the lower stratosphere (just above the jet maximum). The mean zonal winds in the CCC GCM do show an improvement in the upper troposphere upon inclusion of this parametrization but only in the Northern Hemisphere. NCAR has demonstrated more success in solving this problem by means of refinements to the treatment of radiative transfer in the CCM (Pitcher et al., 1983; Ramanathan et al., 1983).

From another point of view, Wallace et al. (1983) show that the simulation of both excessively strong jets in the upper troposphere and anomalously low heights over Europe in winter may be related to the use of incorrect orographic forcing. They were led to this conclusion by examining the systematic error of the ECMWF model, and found that the use of enhanced ("envelope") topography led to a reduction of these errors.

Palmer et al. (1986) and Slingo and Pearson (1987) argue that the use of a gravity wave drag parametrization is necessary in a high-resolution GCM. The argument given by Palmer et al. is that low-resolution GCMs are able to simulate reasonably the zonal wind field only because of compensating errors, namely an underestimate of the atmospheric momentum flux convergence, which is offset by a neglect of drag due to orographically generated gravity waves. Thus many low-resolution GCMs do poorly in simulating the Southern Hemisphere surface winds, for in this nearly mountain-free hemisphere an underestimate of the momentum flux is not compensated by an error in the drag.

In the high-resolution (2.5 lat $\times$ 3.75 long. grid) GCM of the British Meteorologi-

cal Office (referred to as BMO), the above-mentioned authors find a number of problems when the gravity wave drag is *not* parametrized, for now the atmospheric momentum flux is well simulated, but the total drag is not. These problems include excessively deep Aleutian and Icelandic lows in winter, accompanied by a severe northeastward displacement of the latter and by overly large westerly surface winds over North America, the north Atlantic and Europe. In addition, the upper-level zonal wind field (polar night jet) is too strong, and the winter-time Pacific storm track (as seen in the 500-mb filtered variance) is displaced so far eastward that it lies over the Canadian West Coast. On the other hand, the Southern Hemisphere surface wind field is well simulated in this high-resolution GCM. Palmer et al. and Slingo and Pearson demonstrate that the only way to improve the simulation of the Northern Hemisphere without degrading the already good simulation of the Southern Hemisphere is to take into account the missing drag via the parametrization of gravity waves.

The nature of the errors in the momentum field in the GLAS GCM is quite different than in the version of the BMO high-resolution GCM without a gravity wave parametrization. Whereas the BMO GCM makes significant errors in the surface winds and in the mid-level, filtered height variance in the Northern Hemisphere, the upper-level zonal wind errors are modest. In contrast, the upper-level zonal wind errors in the GLAS GCM are quite significant (the jets do not close) in *both* hemispheres and in all seasons, whereas the simulation of sea-level pressure and mid-level variances in the Northern Hemisphere is considerably more realistic in the GLAS GCM. (For instance, both the position and intensity of the Icelandic Low are far more accurate in the GLAS GCM, as is the geographical pattern of the 500-mb band-pass height variance.) In the Southern Hemisphere, the surface wind is in fact quite well simulated by the GLAS GCM (as by the BMO GCM), in distinct contrast with the results from an earlier version of the GLAS model that was referred to by Palmer et al. The lack of a hemispheric dependence in the upper-level zonal wind error in the GLAS GCM and its generally successful simulation of the surface fields in the Northern Hemisphere imply that a parametrization of gravity wave drag would not significantly improve the simulation with this GCM. The overall realism of the vertically integrated total momentum flux convergence in the GLAS GCM (see Fig. 15) confirms this. In terms of the distinct differences between "low resolution" and "high resolution" models posited by Palmer et al., the GLAS GCM is best characterized as having intermediate resolution.

The sensitivity of the simulation of the polar night jet to horizontal diffusion in the stratosphere has been explored by Boville (1984, 1985) in the context of the spectral (R15) NCAR CCM, using versions with 9 and 14 levels. The successful simulation of the polar night jet in this GCM is degraded by omitting horizontal diffusion selectively on a scale-dependent basis. When the diffusion acting on all the lower wavenumbers (defined as the bottom half of the rhomboid in wavenumber space) is omitted, the extent of the degradation is severe. Omitting the diffusion acting on only the zonally symmetric components (for example) leads to a much less extensive change. Artificially decreasing the eddy radiative damping leads to much the same result. In the GLAS GCM, the only horizontal diffusion present (besides the Fourier filtering needed near the pole) is the Shapiro filtering. The results of Boville suggest that the

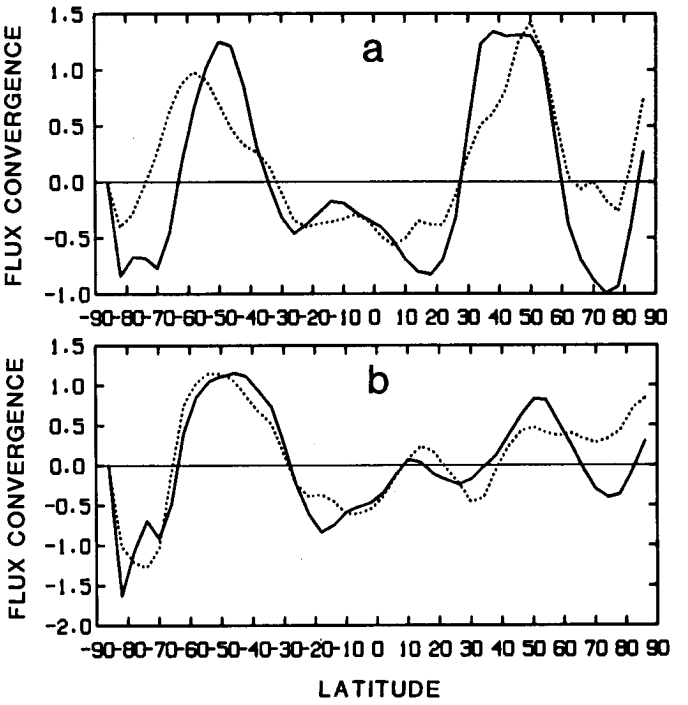

Fig. 15 Vertical integral of the zonally averaged convergence of total momentum flux, $-(1/a\cos^2\theta)\,\partial/\partial\theta(uv\cos^2\theta)$ where θ is the latitude and a is the earth's radius. The solid line is from ECMWF-7 data, the dashed line from the GCM. (a) DJF and (b) JJA. Units: 0.1 kg m^{-1} s^{-2}.

introduction of further horizontal diffusion at the upper levels might improve the simulation of the zonal wind field. It is not clear, however, that such an additional diffusion would be justified on physical grounds.

Another error in the simulation is the excessive rainfall over the continents in local summer. It seems likely that unrealistic latent heating due to precipitation, especially in the tropics, could also be contributory to the deficiencies in the simulation of the extratropical stationary eddies (reported in SS2). It is noteworthy that the stationary eddies are particularly unrealistic during northern summer. Such a sensitivity in the mid-latitude response to changes in tropical heating has been reported recently in high-resolution linear calculations by Jacqmin and Lindzen (1985), and Lin (1983) discusses the role of high-latitude heating in forcing stationary waves in northern summer. The similarity of the GLAS GCM's precipitation errors to those of other, quite different, GCMs suggests a common cause.

It should be recalled that this GCM has demonstrated a certain success in simulating the short-term (monthly to seasonal) effects of changes in SST (Moura and Shukla, 1981; Shukla and Wallace, 1983; Fennessy et al., 1985; Shukla and Fennessy, 1988). The deficiencies discussed in this paper did not interfere with these shorter-term sensitivity studies apparently because the transients of importance in the sensitivity studies do not strongly interact with the GCM's climate drift (Shukla and

Fennessy, 1988). It is clear, then, that the ability to simulate the annual mean and seasonal cycle well is a more stringent requirement for a GCM than the ability to give reasonable results in monthly to seasonal sensitivity studies.

In this paper we have tried to resist the temptation to dwell on the obvious similarities between the GCM's simulation and the observations. Rather we have attempted to emphasize the errors, since it is only through the elimination of these errors that progress in understanding and predicting the atmosphere can come about. While we have not been able to unambiguously identify the precise elements of the formation of this GCM that are responsible for the errors in the simulation of the seasonal cycle, the clear identification of these errors is a significant first step. We hope this effort will stimulate other modelling groups to report more fully on their simulations of the seasonal cycle.

The question of just how much GCMs differ from one another in their simulations of the seasonal cycle is an important one, and in the future we plan to extend the present work to a number of other GCMs.

Acknowledgements

We owe special thanks to many people for their help and encouragement in completing this project: M. Halem, E. Kalnay, L. Marx, Y. Mintz, D. Randall and Y. Sud. The programming support of J. Ardizzone and the drafting work of L. Rumburg are also greatly appreciated. The comments of the anonymous referees are appreciated.

References

ARAKAWA, A. 1969. Parameterization of cumulus convection. Proc. WMO/IUGG Symp. on Numerical Prediction in Tokyo, IV8, 1–6.

———. 1972. Design of the UCLA general circulation model. Numerical Simulation of Weather and Climate. Tech. Rep. No. 7, Dep. of Meteorology, UCLA.

——— and V.R. LAMB. 1977. Computational design of the basic dynamical processes of the UCLA general circulation model. In: *Methods in Computational Physics*, Vol. 17, J. Chang (Ed.), Academic Press, New York, pp. 173–265.

——— and M.J. SUAREZ. 1982. Vertical differencing of the primitive equations in sigma coordinates. *Mon. Weather Rev.*, **111**: 34–35.

ARKIN, P.A.; V.E. KOUSKY, J.E. JANOWIAK and E.A. O'LENIC. 1986. Atlas of the tropical and subtropical circulation derived from National Meteorological Center operational analysis. NOAA Atlas No. 7.

BENGTSSON, L.; M. KANAMITSU, P. KALLBERG and S. UPPALA. 1982. FGGE 4-dimensional data assimilation at ECMWF. *Bull. Am. Meteorol. Soc.* **63**: 29–43.

BOER, G.J.; N.A. MCFARLANE, R. LAPRISE, J.D. HENDERSON and J.-P. BLANCHET. 1984a. The Canadian Climate Centre general circulation model. ATMOSPHERE-OCEAN, **22**: 397–429.

———; ——— and ———. 1984b. The climatology of the Canadian Climate Centre general circulation model as obtained from a five-year simulation. ATMOSPHERE-OCEAN, **22**: 430–473.

BORGER, G.R. and A.D. VERNEKAR. 1988. Validation of outgoing longwave radiation in a general circulation model. *Mon. Weather Rev.* **116**: 106–119.

BOVILLE, B.A. 1984. The influence of the polar night jet on the tropospheric circulation in a GCM. *J. Atmos. Sci.* **41**: 1132–1142.

———. 1985. The influence of wave damping on the winter lower stratosphere. *J. Atmos. Sci.* **42**: 904–916.

BRITISH METEOROLOGICAL OFFICE. 1977. Monthly ice charts. Meteorological Office, London Road, Bracknell, Berkshire.

CHERVIN, R.M. 1986. Interannual variability and seasonal climate predictability. *J. Atmos. Sci.* **43**: 233–251.

DAVIES, R. 1982. Documentation of the solar radia-

tion code in the GLAS GCM. NASA Tech. Memo. 83961, [NTIS-N82-30779] 57 pp.

DEARDORFF, J.W. 1972. Parameterization of the planetary boundary layer for use in general circulation models. *Mon. Weather Rev.* **100**: 93–106.

FENNESSY, M.J.; L. MARX and J. SHUKLA. 1985. General circulation model sensitivity to 1982–83 equatorial Pacific sea surface temperature anomalies. *Mon. Weather Rev.* **113**: 858–864.

HANSEN, J.; G. RUSSELL, D. RIND, P. STONE, A. LACIS, S. LEBEDEFF, R. RUEDY and L. TRAVIS. 1983. Efficient three-dimensional global models for climate studies: Models I and II. *Mon. Weather Rev.* **111**: 609–662.

HOREL, J.D. 1982. On the annual cycle of the tropical Pacific atmosphere and ocean. *Mon. Weather Rev.* **110**: 1863–1878.

HSU, C.-P.F. and J.M. WALLACE. 1976a. The global distribution of the annual and semiannual cycles in precipitation. *Mon. Weather Rev.* **104**: 1093–1101.

——— and ———. 1976b. The global distribution of the annual and semiannual cycles in sea level pressure. *Mon. Weather Rev.* **104**:1597–1601.

JACQMIN, D. and R.S. LINDZEN. 1985. The causation and sensitivity of the northern winter Planetary waves. *J. Atmos. Sci.* **42**: 724–745.

JAEGER, L. 1976. Monatskarten des Niederschlags fur die ganz Erde. *Berichte des Deutschen Wetterdienstes*, 18, No. 139. Im Selbsverlag des Deutschen Wetterdienstes, Offenbach, W. Germany.

KITOH, A. and T. TOKIOKA. 1986. A simulation of the tropospheric general circulation with the MRI atmospheric general circulation model. Part II: The July performance. *Papers Meteorolo. Geophys.* **37**: 145–168.

——— and ———. 1987. A simulation of the tropospheric general circulation with the MRI atmospheric general circulation model. Part III: The Asian summer monsoon. *J. Meteorol. Soc. Jpn*, **65**: 167–187.

KOUSKY, V.E. and S. SRIVATSANGAM. 1983. The seasonal cycle over the United States and Mexico. *Mon. Weather Rev.* **111**: 165–171.

KRISHNAMURTHY, V. 1982. The documentation of the Wu-Kaplan radiation parameterization. NASA Tech. Memo. 83926, 93 pp.

KUSHNIR, Y. and S.K. ESBENSEN. 1986a. Northern Hemisphere wintertime variability in a two-level general circulation model. Part I: Statistical characteristics of short and long time-scale disturbances. *J. Atmos. Sci.* **43**: 2968–2984.

——— and ———. 1986b. Northern Hemisphere wintertime variability in a two-level general circulation model. Part II: The maintenance of short and long time-scale disturbances. *J. Atmos. Sci.* **43**: 2985–2998.

LAU, N.-C. 1981. A diagnostic study of recurrent meteorological anomalies appearing in a 15-year simulation with a GFDL general circulation model. *Mon. Weather Rev.* **109**: 2287–2311.

———. 1985. Modeling the seasonal dependence of the atmospheric response to observed El Niños in 1962–1976. *Mon. Weather Rev.* **113**: 1970–1996.

LIN, B.-D. 1983. The behavior of stationary waves and the summer monsoons. *J. Atmos. Sci.* **40**: 1163–1177.

MANABE, S. and J.L. HOLLOWAY, JR. 1975. The seasonal variation of the hydrological cycle as simulated by a global model of the atmosphere. *J. Geophys. Res.* **80**: 1617–1659.

——— and D.C. HAHN. 1981: Simulation of atmospheric variability. *Mon. Weather Rev.* **109**: 2260–2286.

——— and R.J. STOUFFER. 1979. A CO_2-climate sensitivity study with a mathematical model of the global climate. *Nature*, **282**: 491–493.

——— and ———. 1980. Sensitivity of a global climate model to an increase of CO_2 concentration in the atmosphere. *J. Geophys. Res.* **85**: 5529–5554.

———; K. BRYAN, and M.J. SPELMAN. 1979. A global ocean-atmosphere climate model with seasonal variation for future studies of climate sensitivity. *Dyn. Atmos. Ocean.* **3**: 393–426.

MINTZ, Y. and V. SERAFINI. 1981. Monthly normal global fields of soil moisture and land-surface evapotranspiration. Int. Symp. on Variations in the Global Water Budget, 10–15 August 1981, Oxford, England.

MITCHELL, J.F.B. and J.A. BOLTON. 1982. Some differences between the MET 0 20 5 and 11 layer model annual cycle integrations. Proc. Workshop on Intercomparison of Large-Scale Models used for Extended Range Forecasts, European Centre for Medium Range Weather Forecasts, (ECMWF) Reading, England, pp. 193–223.

MOENG, C.-H. and D.A. RANDALL. 1982. The radiative impact of cumulus cloudiness in a general circulation model. NASA Tech. Memo. 84962, 19 pp.

MOURA, A.D. and J. SHUKLA. 1981. On the dynamics of droughts in northeast Brazil: Observations, theory and numerical experiments with a general circulation model. *J. Atmos. Sci.* **38**: 2653–2675.

OTTO-BLIESNER, B.L.; G.W. BRANSTATOR and D.D. HOUGHTON. 1982. A global low order spectral general circulation model. Part I: Formulation and seasonal climatology. *J. Atmos. Sci.* **39**: 929–948.

PALMER, T.N.; G.J. SHUTTS and R. SWINBANK. 1986. Alleviation of a systematic westerly bias in general circulation and numerical weather prediction models through an orographic gravity wave drag parameterization. *Q.J.R. Meteorol. Soc.* **112**: 1001–1039.

PITCHER, E.J.; R.C. MALONE, V. RAMATHANAN, M.L. BLACKMON, K. PURI and W. BOURKE. 1983: January and July simulations with a spectral general circulation model. *J. Atmos. Sci.* **40**: 580–604.

POSEY, J.W. and P.F. CLAPP. 1964. Global distribution of normal surface albedo. *Geof. Int.* **4**: 33–43.

POTTER, G.L. and W.L. GATES. 1984. A preliminary intercomparison of the seasonal response of two atmospheric climate models. *Mon. Weather Rev.* **112**: 909–917.

RAMANATHAN, V.; E.J. PITCHER, R.C. MALONE and M.L. BLACKMON. 1983. The response of a spectral general circulation model to refinements in radiative processes. *J. Atmos. Sci.* **40**: 605–630.

RANDALL, D.A. 1982. Monthly and seasonal simulations with the GLAS climate model. Proc. Workshop on Intercomparison of Large-Scale Models used for Extended Range Forecasts, ECMWF, Reading, England, pp. 107–166.

———; J.A. ABELES and T.G. CORSETTI. 1985. Seasonal simulations of the planetary boundary layer and boundary-layer stratocumulus clouds with a general circulation model. *J. Atmos. Sci.* **42**: 641–676.

RASMUSSON, E.M. and J.M. WALLACE. 1983. Meteorological aspects of the El Niño/Southern Oscillation. *Science*, **222**: 1195–1202.

SHUKLA, J. and M.J. FENNESSY. 1988. Prediction of time-mean atmospheric circulation and rainfall: Influence of Pacific sea surface temperature anomaly. *J. Atmos. Sci.* **45**: 9–28.

——— and J.M. WALLACE. 1983. Numerical simulation of the atmospheric response to equatorial Pacific sea surface temperature anomalies. *J. Atmos. Sci.* **40**: 1613–1630.

———; D. STRAUS, D. RANDALL, Y. SUD and L. MARX. 1981. Winter and summer simulations with the GLAS climate model. NASA Tech. Memo. 83866, [NTIS n82 18807] 282 pp.

SLINGO, A. and D.W. PEARSON. 1987. A comparison of the impact of an envelope orography and of a parametrization of orographic gravity-wave drag on model simulations. *Q.J.R. Meteorol. Soc.* **113**: 847–870.

SOMERVILLE, R.C.J.; P.H. STONE, M. HALEM, J.E. HANSEN, J.S. HOGAN, L.M. DRUYAN, G. RUSSELL, A.A. LACIS, W.J. QUIRK. and J. TENENBAUM. 1974. The GISS model of the global atmosphere. *J. Atmos. Sci.* **31**: 84–117.

STRAUS, D.M. 1983. On the role of the seasonal cycle. *J. Atmos. Sci.* **40**: 303–313.

———. 1988. The seasonal cycle of energetics from the GLAS/UMD climate GCM. NASA Tech. Memo., NASA/Goddard Space Flight Center, Greenbelt, Md., 44 pp.

——— and J. SHUKLA. 1988. A comparison of a GCM simulation of the seasonal cycle of the atmosphere with observations. Part II: Stationary waves and transient fluctuations. ATMOSPHERE-OCEAN, **26**: 575–607.

SUD, Y.C. and A. MOLOD. 1987. Influence of recent improvements in the parameterization of convection in the GLA GCM and the roles of dry convection and cloud radiation feedback, submitted to *Monthly Weather Review*.

TENENBAUM. 1982. Integrated and spectral energetics studies of the GLAS general circulation model. *Mon. Weather Rev.* **110**: 962–980.

TOKIOKA, T.; A. KITOH, I. YAGAI and K. YAMAZAKI. 1985. A simulation of the tropospheric general circulation with the MRI atmospheric general circulation model. Part I: The January performance. *J. Meteorol. Soc. Jpn*, **63**: 749–778.

———; K. YAMAZAKI and A. KITOH. 1986. Mean statistics of the tropospheric MRI·GCM-I based on 12-year integration. Tech. Rep. of the Meteorol. Res. Inst. No. 20, Tsukuba, 314 pp.

TRENBERTH, K.E. 1979. Interannual variability of the 500 mb zonal mean flow in the Southern Hemisphere. *Mon. Weather Rev.* **107**: 1515–1524.

———. 1984. Interannual variability of the Southern Hemisphere circulation: Representativeness of the year of the Global Weather Experiment. *Mon. Weather Rev.* **112**: 108–123.

———. 1987. The zonal mean westerlies over the Southern Hemisphere. *Mon. Weather Rev.* **115**: 1528–1533.

VAN LOON, H. 1972a. Temperature in the Southern Hemisphere. *In*: Meteorology of the Southern Hemisphere. Meteor. Monogr. No. 35, C.W. Newton (Ed.), Am. Meteorol. Soc. pp. 25–58.

———. 1972b. Pressure in the Southern Hemisphere. Ibid., pp. 59–86.

——— and J.C. RODGERS. 1984a. The yearly wave in pressure and zonal geostrophic wind at sea

level on the Southern Hemisphere and its interannual variability. *Tellus*, **36**: 348–354.

——— and ———. 1984b. Interannual variations in the half-yearly cycle of pressure gradients and zonal wind at sea level on the Southern Hemisphere. *Tellus*, **36A**: 76–86.

WALLACE, J.M.; S. TIBALDI and A.J. SIMMONS. 1983. Reduction of systematic forecast errors in the ECMWF model through introduction of an envelope topography. *Q.J.R. Meteorol. Soc.* **109**: 683–717.

WETHERALD, R.T. and S. MANABE. 1981. Influence of seasonal variation upon the sensitivity of a model climate. *J. Geophys. Res.* **86**: 1194–1204.

WHITE, G.H. and J.M. WALLACE. 1978. The global distribution of the annual and semiannual cycles in surface temperature. *Mon. Weather Rev.* **106**: 901–906.

WISENET, D.R. and D. MATSON. 1976. A possible forecasting technique for winter snow cover in the northern Hemisphere and Eurasia. *Mon. Weather Rev.* **104**: 828–835.

ZWALLY, H.J.; J.C. COMISO, C.L. PARKINSON, W.J. CAMPBELL, F.D. CARSEY and P. GLOERSEN. 1983. Antarctic sea ice, 1973–1976: Satellite passive microwave observations. NASA SP-459, National Aeronautics and Space Administration Washington, D.C.

ZWIERS, F.W. and G.J. BOER. 1987. A comparison of climates simulated by a general circulation model when run in the annual cycle and perpetual modes. *Mon. Weather Rev.* **115**: 2626–2644.